

NON-UNIFORM QUANTUM FOURIER TRANSFORM

JUNAID AFTAB, YUEHAW KHOO, AND HAIZHAO YANG

ABSTRACT. The Discrete Fourier Transform (DFT) is fundamental to the analysis of uniformly sampled signals; however, many practical settings involve non-uniform sampling, necessitating the Non-Uniform Discrete Fourier Transform (NUDFT). While efficient quantum algorithms for the standard DFT are well established, a systematic treatment of the non-uniform case remains limited. We present a quantum algorithm for the Non-Uniform Quantum Fourier Transform (NUQFT) based on a low-rank approximation. This factorization is translated into an explicit quantum algorithm, yielding an ϵ -accurate block encoding with rigorously controlled errors arising from both classical truncation and quantum implementation. The resulting complexity scales polylogarithmically in the target precision, quadratically in the number of qubits, and logarithmically in a geometry-dependent conditioning parameter induced by the non-uniform sampling grid. Numerical experiments validate the predicted low-rank truncation behavior, confirm the mild precision dependence on the geometry parameter, and demonstrate small-scale implementations of the key unitary primitives.

1. INTRODUCTION

The Discrete Fourier Transform (DFT), introduced by Gauss and later popularized by Cooley and Tukey [1], provides a framework for computing Fourier coefficients from uniformly sampled data and underpins applications in signal processing, data compression, and numerical solutions of differential equations (see, e.g., [2–4]). In practice, however, uniform sampling is often infeasible due to physical constraints, adaptive sampling, or irregular geometries. The Non-Uniform Discrete Fourier Transform (NUDFT) [5] generalizes the DFT to arbitrary sampling grids, enabling spectral analysis on non-uniform data and irregular computational domains, with important applications in imaging and numerical methods (see, e.g., [6, 7]). Consequently, a broad class of efficient classical algorithms for computing the NUDFT has been developed (see, e.g., [8–16]).

The Quantum Fourier Transform (QFT) (see, e.g., [17–19]) is the quantum analogue of the DFT and a central primitive in quantum algorithm design. It appears as a core subroutine in many quantum algorithms, including Shor’s factoring algorithm [20], Kitaev’s quantum phase estimation [21], quantum linear systems algorithms [22], ground-state energy estimation [23], and quantum arithmetic [24, 25]. Recent work has explored several extensions of the QFT, such as multi-dimensional extensions, approximate implementations with reduced gate complexity, topology-aware variants adapted to specific hardware architectures, and fault-tolerant constructions for error-corrected quantum computation (see, e.g., [26–31]). In contrast, quantum algorithms for Fourier transforms on non-uniform grids, particularly in a fully quantum setting, remain relatively underexplored.

In this work, we propose a quantum algorithm for the NUDFT, termed the Non-Uniform Quantum Fourier Transform (NUQFT). The construction builds on the low-rank approximation framework of Antolín and Townsend [14] and translates this decomposition into an explicit quantum algorithm. The factorization is implemented using Quantum Signal Processing (QSP) [32, 33] together with the Linear Combination of Unitaries (LCU) [34] algorithms. This yields an explicit block encoding [33] of the NUDFT matrix to arbitrary precision, with controlled approximation errors stemming from both the classical low-rank truncation and its quantum realization. We also provide explicit gate-level resource estimates for the resulting circuits under standard oracle access assumptions for non-uniform sampling points.

1.1. Problem Statement. Let $\{x_j\}_{j=0}^{N-1} \subseteq \mathbb{C}$ denote samples taken at non-uniform locations $\{t_j\}_{j=0}^{N-1} \subseteq \mathbb{T}$, viewed as a discrete representation of an underlying function $f : \mathbb{T} \rightarrow \mathbb{C}$. The Non-Uniform Discrete Fourier Transform (NUDFT) of $\{x_j\}_{j=0}^{N-1}$, evaluated at non-uniform frequencies $\{\omega_k\}_{k=0}^{N-1} \subseteq \mathbb{R}$, is defined by

$$\begin{pmatrix} X_0 \\ X_1 \\ \vdots \\ X_{N-1} \end{pmatrix} = \begin{pmatrix} e^{-i\omega_0 t_0} & e^{-i\omega_0 t_1} & \dots & e^{-i\omega_0 t_{N-1}} \\ e^{-i\omega_1 t_0} & e^{-i\omega_1 t_1} & \dots & e^{-i\omega_1 t_{N-1}} \\ \vdots & \vdots & \ddots & \vdots \\ e^{-i\omega_{N-1} t_0} & e^{-i\omega_{N-1} t_1} & \dots & e^{-i\omega_{N-1} t_{N-1}} \end{pmatrix} \begin{pmatrix} x_0 \\ x_1 \\ \vdots \\ x_{N-1} \end{pmatrix}. \quad (1)$$

In the literature, Equation (1) is known as the Type-III NUDFT, and the matrix is denoted by F_{III} . Two special cases arise depending on whether the sampling locations and frequency points are uniform or non-uniform:

- (I) **Type-I NUDFT.** The sequence $\{t_j\}_{j=0}^{N-1}$ is sampled uniformly at points $t_j = 2\pi j/N$, but the sequence $\{\omega_k\}_{k=0}^{N-1}$ is sampled at potentially non-uniform points. We denote the corresponding matrix as F_{I} .
- (II) **Type-II NUDFT.** The sequence $\{t_j\}_{j=0}^{N-1}$ is sampled at potentially non-uniform points $\{t_j\}_{j=0}^{N-1}$, but the sequence $\{\omega_k\}_{k=0}^{N-1}$ is uniformly spaced with $\omega_k = k$. We denote the corresponding matrix as F_{II} .

We argue in Section 3 that it suffices to develop a quantum algorithm for the Type-II case. Hence, we focus on developing a quantum algorithm for the Type-II NUDFT in this work.

1.2. Summary of Results. Let $N = 2^n$ for $n \geq 1$. Antolín and Townsend [14] approximate F_{II} by $F_{\text{II}} \approx \sum_{r=0}^{K-1} D_{\vec{u}_r} F D_{\vec{v}_r}$. (See later sections for the more general form of F_{II} .) Here, F is the standard discrete Fourier transform matrix, and $D_{\vec{u}_r}, D_{\vec{v}_r}$ are diagonal matrices. Assuming oracle access to the sampling points $\{t_j\}_{j=0}^{2^n-1}$, our algorithm constructs quantum circuits $U_{\vec{u}_r}$ and $U_{\vec{v}_r}$ that provide block encodings of $D_{\vec{u}_r}$ and $D_{\vec{v}_r}$. Combining these with the standard block encoding of F and applying the Linear Combination of Unitaries (LCU) technique implements $\sum_{r=0}^{K-1} D_{\vec{u}_r} F D_{\vec{v}_r}$. We provide non-asymptotic gate-count estimates (Theorem 24), resource bounds for achieving ϵ -accurate block encodings (Theorem 28), and simplified complexity estimates (Corollary 29), including explicit gate counts sufficient to obtain an ϵ -accurate block encoding.

Result 1 (Asymptotic Version of Theorem 24 based on Corollary 29). Let $\epsilon > 0$ and let $n \in \mathbb{N}$ with $N = 2^n$. There exists a quantum circuit, V_{II} , that implements an ϵ -accurate block-encoding of F_{II} . Let

$$L_{n,\epsilon} := n + \log(1/\epsilon), \quad \kappa := \max_j (1 - (y_j^*)^2)^{-1/2}, \quad (2)$$

where $y_j^* \in (-1, 1)$ are points determined by the non-uniform sampling points. The circuit uses $\mathcal{O}(L_{n,\epsilon} + \log(1 + \kappa L_{n,\epsilon}))$ qubits, $\mathcal{O}(n + \log L_{n,\epsilon})$ Hadamard gates, $\mathcal{O}(L_{n,\epsilon}^2 + \log(1 + \kappa L_{n,\epsilon}))$ CNOT gates, $\mathcal{O}(L_{n,\epsilon} + \log(1 + \kappa L_{n,\epsilon}))$ Toffoli and σ_X gates, and $\mathcal{O}(n^2 + L_{n,\epsilon}^2 + \log(1 + \kappa L_{n,\epsilon}))$ single-qubit controlled rotation gates. The circuit depth is $\mathcal{O}(L_{n,\epsilon} \log L_{n,\epsilon} + \log(1 + \kappa L_{n,\epsilon}))$.

The resource bounds in Result 1 depend on three parameters: the number of qubits n , the target accuracy ϵ , and the geometry-dependent quantity κ . The accuracy parameter enters only through the logarithmic factor $\log(1/\epsilon)$, appearing additively with n in the composite parameter $L_{n,\epsilon}$. Hence increasing precision affects gate counts and circuit depth only polylogarithmically. The quadratic dependence on n originates from the implementation of the quantum Fourier transform. All remaining gate counts scale as $L_{n,\epsilon} \log L_{n,\epsilon}$, except for a single $L_{n,\epsilon}^2$ term, up to additional logarithmic factors depending on κ . The parameter κ , capturing conditioning from the non-uniform sampling points, contributes only through logarithmic factors of the form $\log(1 + \kappa L_{n,\epsilon})$. In particular, no

resource depends polynomially on κ , and its contribution remains subdominant whenever κ grows at most exponentially in n or $\log(1/\epsilon)$.

1.3. Related Works. In contrast to the extensive literature on the QFT, little work has addressed quantum implementations of Fourier transforms on non-uniform grids. To the best of our knowledge, the closest related proposal is due to Gyongyosi and Imre [35]. That work introduces a method termed ‘‘Quantum-SVD,’’ in which a standard QFT on a uniform grid is followed by a classical singular value decomposition–based interpolation step to approximate Fourier coefficients at non-uniform sampling points. As a result, the procedure is hybrid: the Fourier transform is quantum, while the handling of non-uniformity is performed classically. By contrast, the approach developed here provides a fully quantum implementation based on a block-encoding framework. Our work can also be placed in the broader context of efforts to develop circuit-level quantum analogues of classical integral transforms, including the quantum wavelet transform [36, 37], quantum Laplace transform [38, 39], quantum Hilbert transform [40, 41], quantum cosine transform [42, 43], quantum Chebyshev transform [44], and quantum Hermite transform [45].

1.4. Organization. The remainder of this paper is organized as follows. Section 2 reviews the necessary preliminaries, including the discrete and quantum Fourier transforms, as well as other quantum algorithmic primitives relevant to this study. Section 3 reviews the low-rank approximation approach to the non-uniform discrete Fourier transform. Section 4 presents our quantum algorithm, and Section 5 provides the corresponding error analysis. Section 6 presents some numerical results. Finally, Section 7 offers concluding remarks and discusses potential directions for future work.

Acknowledgments. J. Aftab was supported by NSF DMS-2231533. Y. Khoo was partially funded by NSF DMS-2339439, DOE DE-SC0022232, DARPA The Right Space HR0011-25-9-0031, and a Sloan research fellowship. H. Yang was partially funded by NSF under awards IIS-2520978, GEO/RISE-5239902, the Office of Naval Research Award N00014-23-1-2007, DOE (ASCR) Award DE-SC0026052, and the DARPA D24AP00325-00.

2. PRELIMINARIES

This section presents the necessary preliminary material. Section 2.1 introduces the notation used throughout the paper. Section 2.2 reviews the Quantum Fourier Transform (QFT). Finally, Section 2.3 summarizes the quantum algorithmic primitives that form the foundation of the proposed method.

2.1. Notation. We briefly discuss the main notation used throughout this work.

2.1.1. Standard Notation. Let \mathbb{R} , \mathbb{C} , and \mathbb{N} denote the sets of real, complex and natural numbers, respectively. Let \mathbb{T} denote the 1-dimensional torus (i.e., the unit circle) identified with the interval $[0, 1]$ with its endpoints identified. If $f, g : \mathbb{N} \rightarrow \mathbb{R}^+$ are non-negative functions, we use the following standard notation from complexity theory:

- (1) $f(n) = \mathcal{O}(g(n))$ if and only if there exists a constant $C > 0$ and an integer $N \in \mathbb{N}$ such that $f(n) \leq Cg(n)$ for all $n \geq N$.
- (2) $f(n) = \Omega(g(n))$ if and only if there exists a constant $C > 0$ and an integer $N \in \mathbb{N}$ such that $f(n) \geq Cg(n)$ for all $n \geq N$.
- (3) $f(n) = \Theta(g(n))$ if and only if $f(n) = \mathcal{O}(g(n))$ and $f(n) = \Omega(g(n))$.

For $r \in \mathbb{N} \cup \{0\}$, $T_r(x)$ denotes the degree- r Chebyshev polynomial of the first-kind on $[-1, 1]$ defined recursively by $T_0(x) = 1$, $T_1(x) = x$ and

$$T_r(x) = 2xT_{r-1}(x) - T_{r-2}(x), \quad r \geq 2. \tag{3}$$

Similarly, $U_r(x)$ denotes the degree- r Chebyshev polynomial of the second-kind on $[-1, 1]$ defined recursively by $U_0(x) = 1, U_1(x) = 2x$ and

$$U_r(x) = 2xU_{r-1}(x) - U_{r-2}(x), \quad r \geq 2. \quad (4)$$

2.1.2. Linear Algebra Notation. Vectors in \mathbb{R}^n or \mathbb{C}^n are denoted by lowercase Roman letters with an overhead arrow. The linear algebra notation used throughout this paper is summarized below:

- (1) $\|\vec{x}\|_1$ denotes the 1-norm of a vector \vec{x} . Similarly, $\|\vec{x}\|_\infty$ denotes the ∞ -norm of \vec{x} .
- (2) $\|A\|$ denotes the spectral norm of a matrix A , defined as its largest singular value.
- (3) $\|A\|_{\max}$ denotes the maximum absolute value among the entries of A .
- (4) The symbol \circ denotes the elementwise (Hadamard) product, acting entry-wise on vectors or matrices of the same dimensions.
- (5) If \vec{x} is a vector and f is a function, then $f(\vec{x})$ denotes the componentwise application of f to \vec{x} .

2.1.3. Quantum Computing Notation. A single-qubit quantum state is represented by a unit vector in \mathbb{C}^2 . In Dirac's notation, such a state is written as $|v\rangle$ and referred to as a *ket*, while its conjugate transpose, denoted $\langle v|$, is called a *bra*. A single-qubit quantum gate is a unitary operator in $\mathbb{C}^{2 \times 2}$. Standard examples include the Pauli matrices:

$$\sigma_X = \begin{pmatrix} 0 & 1 \\ 1 & 0 \end{pmatrix}, \quad \sigma_Y = \begin{pmatrix} 0 & -i \\ i & 0 \end{pmatrix}, \quad \sigma_Z = \begin{pmatrix} 1 & 0 \\ 0 & -1 \end{pmatrix}. \quad (5)$$

Single-qubit rotation gates about the X , Y , and Z axes are defined as follows:

$$e^{-i\theta\sigma_X} = \begin{pmatrix} \cos \theta & -i \sin \theta \\ -i \sin \theta & \cos \theta \end{pmatrix}, \quad e^{-i\theta\sigma_Y} = \begin{pmatrix} \cos \theta & -\sin \theta \\ \sin \theta & \cos \theta \end{pmatrix}, \quad e^{-i\theta\sigma_Z} = \begin{pmatrix} e^{-i\theta} & 0 \\ 0 & e^{i\theta} \end{pmatrix}. \quad (6)$$

We also denote the quantum gates $e^{-i\theta\sigma_X}$, $e^{-i\theta\sigma_Y}$, and $e^{-i\theta\sigma_Z}$ as $R_X(\theta)$, $R_Y(\theta)$, and $R_Z(\theta)$, respectively. Another important example of a single-qubit gate is the Hadamard gate:

$$H = \frac{1}{\sqrt{2}} \begin{pmatrix} 1 & 1 \\ 1 & -1 \end{pmatrix} = \text{---} \boxed{H} \text{---} \quad (7)$$

A k -qubit quantum state is a unit vector \mathbb{C}^{2^k} and a k -qubit quantum gate is a unitary operator in $\mathbb{C}^{2^k \times 2^k}$. An important example of a k -qubit gate is the k -fold tensor product of Hadamard gates:

$$H^{\otimes k} = \frac{1}{\sqrt{2}} \begin{pmatrix} 1 & 1 \\ 1 & -1 \end{pmatrix}^{\otimes k} = \text{---} \boxed{H^{\otimes k}} \text{---} \quad (8)$$

It is often necessary to construct multi-qubit controlled gates. A generic k -qubit gate, U , controlled on l qubits, is denoted as follows:

$$C^l U = \text{---} \begin{array}{c} \text{---} \text{---} \text{---} \text{---} \\ | \\ \text{---} \text{---} \text{---} \text{---} \\ \boxed{U} \end{array} \text{---} \quad (9)$$

An important example of a two-qubit gate is the CNOT gate, while a three-qubit example is the Toffoli (CCNOT) gate:

$$\text{CNOT} = \begin{pmatrix} 1 & 0 & 0 & 0 \\ 0 & 1 & 0 & 0 \\ 0 & 0 & 0 & 1 \\ 0 & 0 & 1 & 0 \end{pmatrix} = \text{---} \begin{array}{c} \text{---} \\ | \\ \oplus \end{array} \text{---} \quad \text{CCNOT} = \begin{pmatrix} 1 & 0 & 0 & 0 & 0 & 0 & 0 & 0 \\ 0 & 1 & 0 & 0 & 0 & 0 & 0 & 0 \\ 0 & 0 & 1 & 0 & 0 & 0 & 0 & 0 \\ 0 & 0 & 0 & 1 & 0 & 0 & 0 & 0 \\ 0 & 0 & 0 & 0 & 1 & 0 & 0 & 0 \\ 0 & 0 & 0 & 0 & 0 & 1 & 0 & 0 \\ 0 & 0 & 0 & 0 & 0 & 0 & 0 & 1 \\ 0 & 0 & 0 & 0 & 0 & 0 & 1 & 0 \end{pmatrix} = \text{---} \begin{array}{c} \text{---} \\ | \\ \oplus \end{array} \text{---} \quad (10)$$

Note that $\text{CNOT} = C\sigma_X$ and $\text{CCNOT} = C^2\sigma_X$. Single-qubit controlled rotations also play an important role in quantum computation. In particular, the following controlled rotation operation arises in the implementation of the Quantum Fourier Transform.

$$CR_m = \begin{pmatrix} 1 & 0 & 0 & 0 \\ 0 & 1 & 0 & 0 \\ 0 & 0 & 1 & 0 \\ 0 & 0 & 0 & e^{-2\pi i/2^m} \end{pmatrix} = \begin{array}{c} \text{---} \\ \bullet \\ | \\ \boxed{R_m} \\ \text{---} \end{array} \quad (11)$$

2.2. Quantum Fourier Transform. Let $N \in \mathbb{N}$. The Discrete Fourier Transform (DFT) can be interpreted as the linear map $\text{DFT}_N : \mathbb{C}^N \rightarrow \mathbb{C}^N$ given by the matrix whose (j, k) -entry is

$$(\text{DFT}_N)_{jk} = \frac{1}{\sqrt{N}} \omega_N^{jk}, \quad (12)$$

where $\omega_N = e^{-2\pi i/N}$ is a primitive N -th root of unity and $0 \leq j, k \leq N-1$. It is straightforward to verify that DFT_N is a unitary operator. The Quantum Fourier Transform (QFT) is the quantum analogue of the Discrete Fourier Transform and acts on quantum states by implementing DFT_N as a quantum circuit, denoted by U_{QFT} . The algorithm realizes U_{QFT} through a sequence of single-qubit and two-qubit gates based on the following expression:

$$U_{\text{QFT}} |x\rangle = \frac{1}{\sqrt{N}} \sum_{y=0}^{N-1} e^{-2\pi i xy/N} |y\rangle = \frac{1}{\sqrt{N}} \bigotimes_{\ell=0}^{n-1} \left(|0\rangle + e^{-2\pi i \sum_{m=1}^{n-\ell} x_{n-\ell-m}/2^m} |1\rangle \right). \quad (13)$$

The tensor-product form in Equation (13) is important because it reveals a hierarchical dependence: the last output qubit depends on all n input qubits, while earlier outputs depend on progressively fewer qubits. This structure enables a simplified and more efficient circuit implementation. In each of the n iterations in Algorithm 1, a Hadamard gate is applied followed by progressively fewer controlled phase rotations, giving a total of $\mathcal{O}(n^2)$ quantum gates. For a vector of size $N = 2^n$, the QFT has computational complexity $\mathcal{O}(\log^2 N) = \mathcal{O}(n^2)$, offering an exponential speedup over the classical FFT, which requires $\mathcal{O}(N \log N) = \mathcal{O}(n2^n)$ operations.

Algorithm 1: Quantum Fourier Transform (QFT) on an n -qubit register

Input: n -qubit quantum state $|x\rangle = |x_0 x_1 \cdots x_{n-1}\rangle$

Output: QFT-transformed quantum state $U_{\text{QFT}} |x\rangle$

for $\ell \leftarrow 0$ **to** $n-1$ **do**

 Apply Hadamard gate H to qubit $n-\ell$

for $m \leftarrow 2$ **to** $n-\ell$ **do**

 Apply CR_m (Equation (11)) with qubit $n-\ell-m$ (control) and qubit $n-\ell$ (target)

return QFT transformed quantum state $U_{\text{QFT}} |x\rangle$

2.3. Quantum Algorithm Primitives. We review the fundamental algorithmic primitives in quantum computation that underpin this work. In particular, we cover quantum arithmetic, the block encoding framework, quantum signal processing (QSP), and the Linear Combination of Unitaries (LCU) algorithm.

2.3.1. Quantum Arithmetic. We assume that all quantum algorithms take as input a fixed-precision binary number stored in an n -qubit quantum register, denoted $|x\rangle$. The leftmost m qubits encode the integer part, while the remaining $n-m$ qubits encode the fractional part. When necessary, an additional qubit may be introduced to represent the sign of the number. Formally,

$$|x\rangle = |x^{(m-1)}\rangle \otimes \cdots \otimes |x^{(0)}\rangle \otimes |x^{(-1)}\rangle \otimes \cdots \otimes |x^{(m-n)}\rangle, \quad (14)$$

where each $x^{(j)} \in \{0, 1\}$ and the number is represented as

$$x = \underbrace{\sum_{j=0}^{m-1} x^{(j)} 2^j}_{\text{integer part}} + \underbrace{\sum_{j=-1}^{-(n-m)} x^{(j)} 2^j}_{\text{fractional part}}. \quad (15)$$

Quantum algorithms for addition (see, e.g., [24, 46, 47]) and multiplication (see, e.g., [48–50]) have been extensively studied, with circuit complexities of $\mathcal{O}(n)$ for addition and $\mathcal{O}(n^2)$ for multiplication, measured in Toffoli and CNOT gates. Since the NUQFT algorithm considered here has overall complexity $\Omega(n^2)$, it is sufficient to treat addition and multiplication as elementary primitives. See Figure 1 for a quantum oracle U_{AM} that implements both addition and multiplication within a single quantum circuit.

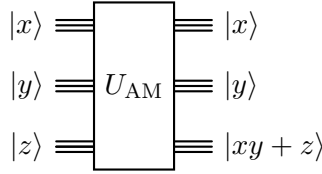


FIGURE 1. Quantum oracle for multiplication and addition implementing $|x\rangle|y\rangle|z\rangle \mapsto |x\rangle|y\rangle|xy + z\rangle$.

Recent work by Burge et al. [51] introduces a reversible quantum algorithm for computing the arcsine function using a quantum adaptation of the CORDIC (COordinate Rotation DIgital Computer) method. The algorithm iteratively approximates $\arcsin(x)$ through a sequence of reversible rotations, enabling efficient implementation on quantum hardware. For a p -bit output, it requires $\mathcal{O}(p)$ qubits and $\mathcal{O}(p^2)$ CNOT gates, with circuit depth scaling as $\mathcal{O}(p \log p)$, and achieves a worst-case approximation error of $\mathcal{O}(2^{-p})$.

Remark 2. The implementation of Burge et al. employs $\mathcal{O}(p)$ additional qubit registers as scratch space for intermediate variables. As this overhead is absorbed into the asymptotic complexity, we use p to denote the ancilla register that stores the final p -bit approximation whenever only the principal p ancillas are being referenced.

2.3.2. Block Encoding. Quantum algorithms for matrix manipulation typically assume that a possibly non-unitary matrix can be embedded as a block of a unitary operator. The block-encoding framework formalizes this approach, enabling linear algebraic operations on a quantum computer by representing a subnormalized matrix A/α as the upper-left block of a unitary. Since such embeddings may be approximate, we recall the following formal definition:

Definition 3. Let $\alpha, \epsilon \in \mathbb{R}^+$. Given $A \in \mathbb{C}^{r \times c}$, we say $U \in \mathbb{C}^{d \times d}$ for $d \geq \max\{r, c\}$ is a (α, ϵ) block encoding of A

$$\|A - \alpha(B_L^\dagger U B_R)\| \leq \epsilon, \quad (16)$$

where $B_L \in \mathbb{C}^{d \times r}$ and $B_R \in \mathbb{C}^{d \times c}$ are the first r and c columns of the identity matrix, respectively.

We will often consider d , r , and c as powers of two. In this case, if $A \in \mathbb{C}^{2^m \times 2^n}$, we will say that a unitary $U \in \mathbb{C}^{2^{m+a} \times 2^{n+a}}$ is a (α, a, ϵ) -block-encoding of A if

$$\|A - \alpha(|0\rangle^a \otimes I_{2^n} U (|0\rangle^a \otimes I_{2^m})\| \leq \epsilon \quad (17)$$

In most cases, we have $m = n$, and this is the case that will be considered below. For ease of notation, we write:

$$U = \begin{pmatrix} A/\alpha & * \\ * & * \end{pmatrix} \quad (18)$$

Let us consider an explicit computation to clarify the notation. Let $A \in \mathbb{C}^{2 \times 2}$ and $\alpha = 1$. In this case, we have

$$(\langle 0| \otimes I_2) U (|0\rangle \otimes I_2) = (I_2 \quad 0) \begin{pmatrix} A & C \\ B & D \end{pmatrix} \begin{pmatrix} I_2 \\ 0 \end{pmatrix} = (I_2 \quad 0) \begin{pmatrix} A \\ B \end{pmatrix} = A. \quad (19)$$

The case when $A \in \mathbb{C}^{2^s \times 2^s}$ for $s > 1$ and $a > 1$ is similar to the above. We will use the following lemma concerning block-encoding products of matrices in our analysis.

Lemma 4 (Lemma 53 in [33]). *If U is an (α, a, δ) -block-encoding of an s -qubit operator A , and V is a (β, b, ϵ) -block-encoding of an s -qubit operator B , then $(I_b \otimes U)(I_a \otimes V)$ is an $(\alpha\beta, a+b, \alpha\epsilon + \beta\delta)$ -block-encoding of AB , where I_a and I_b act on the ancilla qubits of U and V respectively.*

We will also use a result on block-encoding sparse matrices, which can be found in [33, Lemma 48]. For our purposes, it suffices to restrict attention to the case in which A is a sparse 0–1 matrix. The corresponding specialization of this result is stated below.

Lemma 5. *Let $A \in \mathbb{C}^{2^n \times 2^n}$ be a d_r -row-sparse and d_c -column-sparse 0-1 matrix. Suppose that we have access to the following $2(n+1)$ -qubit oracles:*

$$O_r : |i\rangle|k\rangle \mapsto |i\rangle|r_{ik}\rangle, \quad 0 \leq i < 2^n, \quad 0 \leq k < d_r, \quad (20)$$

$$O_c : |l\rangle|j\rangle \mapsto |c_{lj}\rangle|j\rangle, \quad 0 \leq j < 2^n, \quad 0 \leq l < d_c, \quad (21)$$

where r_{ik} is the index of the k -th non-zero entry of the i -th row of A , or if there are fewer than k non-zero entries, then $r_{ik} = k + 2^n$, and similarly c_{lj} is the index of the l -th non-zero entry of the j -th column of A , or if there are fewer than l non-zero entries, then $c_{lj} = l + 2^n$. Additionally, assume we have access to a one-bit oracle

$$O_A : |i\rangle|j\rangle|0\rangle \mapsto |i\rangle|j\rangle|A_{ij}\rangle, \quad 0 \leq i, j < 2^n, \quad (22)$$

where $A_{ij} \in \{0, 1\}$. Then one can implement a $(\sqrt{d_r d_c}, n+3, 0)$ -block-encoding of A with a single use of O_r, O_c , two uses of O_A and additionally $\mathcal{O}(n)$ one-qubit and two-qubit gates, while using $\mathcal{O}(1)$ ancilla qubits (which are discarded before the ϵ -post-selection step).

The proof of Lemma 5 follows the same argument as that of the general result in [33, Lemma 48] and is therefore omitted.

2.3.3. Quantum Signal Processing. Quantum signal processing (QSP) is a framework for implementing polynomial transformations of scalars that are block-encoded in a unitary operator. In particular, QSP constructs 2×2 unitary matrices whose entries are complex polynomials of a real scalar $x \in [-1, 1]$ by composing single-qubit rotations and phase gates. It considers a single-qubit unitary operator that block-encodes $x \in [-1, 1]$ as follows:

$$e^{i \arccos(x) \sigma_X} = \begin{pmatrix} x & i\sqrt{1-x^2} \\ i\sqrt{1-x^2} & x \end{pmatrix}, \quad \theta \in [0, \pi]. \quad (23)$$

For $\varphi = (\varphi_0, \dots, \varphi_\ell)$, QSP implements the following quantum circuit:

$$V_\varphi(x) = e^{i\varphi_0 \sigma_Z} e^{i \arccos(x) \sigma_X} e^{i\varphi_1 \sigma_Z} e^{i \arccos(x) \sigma_X} \dots e^{i \arccos(x) \sigma_X} e^{i\varphi_\ell \sigma_Z}. \quad (24)$$

Polynomial functions realizable by Equation (24) are completely characterized by the following result:

Proposition 6 (Theorem 3 in [33]). *Let $\ell \in \mathbb{N}$ and $x \in [-1, 1]$. There exists $\varphi = (\varphi_0, \varphi_1, \dots, \varphi_\ell) \in \mathbb{R}^{\ell+1}$ such that*

$$V_\varphi(x) = e^{i\varphi_0 \sigma_Z} \prod_{j=1}^{\ell} \left(e^{i \arccos(x) \sigma_X} e^{i\varphi_j \sigma_Z} \right) = \begin{pmatrix} p(x) & iq(x)\sqrt{1-x^2} \\ iq^*(x)\sqrt{1-x^2} & p^*(x) \end{pmatrix} \quad (25)$$

if and only if $p, q \in \mathbb{C}[x]$ such that:

- (i) $\deg(p(x)) \leq \ell$ and $\deg(q(x)) \leq \ell - 1$,
- (ii) $p(x)$ has parity $\ell \bmod 2$ and $q(x)$ has parity $\ell - 1 \bmod 2$ ¹,
- (iii) For all $x \in [-1, 1]$, we have $|p(x)|^2 + (1 - x^2)|q(x)|^2 = 1$.

Example 7. QSP is an important quantum circuit because it enables the implementation of various polynomial transformations. A simple choice of phase factors $(0, \dots, 0) \in \mathbb{R}^{\ell+1}$ ensures that $p(x) = T_\ell(x)$, where $T_\ell(x)$ is the degree- ℓ Chebyshev polynomial of the first kind. We will use this result below. This observation has also recently been used to advocate QSP as a framework for function approximation (see, e.g., [52, 53]).

2.3.4. Linear Combination of Unitaries. The Linear Combination of Unitaries (LCU) algorithm [54] provides a framework for implementing a linear combination of unitary operators on a quantum computer. Let $M \in \mathbb{N}$, and let $\alpha_1, \dots, \alpha_M \in \mathbb{R}$ and U_1, \dots, U_M be unitary operators. The LCU method aims to implement the operator $U = \sum_{j=1}^M \alpha_j U_j$. The algorithm assumes that the following two operators can be implemented. First, it assumes the existence of a state preparation (PREP) oracle:

$$\text{PREP } |0\rangle = \frac{1}{\sqrt{\|\vec{\alpha}\|_1}} \sum_{j=1}^M \sqrt{\alpha_j} |j\rangle, \quad (26)$$

where $\sqrt{\cdot}$ denotes the principal branch of the square root. Second, it assumes that a multi-qubit controlled gate, also called a select (SEL) oracle in the literature, can be implemented:

$$\text{SEL} = \sum_{j=1}^M U_j \otimes |j\rangle \langle j|. \quad (27)$$

Assuming access to the required operators, the LCU algorithm implements the unitary operator $U_{\text{LCU}} = \text{PREP}^\dagger \cdot \text{SEL} \cdot \text{PREP}$. See Figure 2 for the corresponding quantum circuit. If $|\psi\rangle$ denotes an input state, $|0\rangle^{\log M}$ represents $\mathcal{O}(\log M)$ ancilla qubits, we have

$$U_{\text{LCU}} |\psi\rangle |0\rangle^{\log M} = \frac{1}{\|\vec{\alpha}\|_1} \left(\sum_{j=1}^M \alpha_j U_j \right) |\psi\rangle |0\rangle^{\log M} + |\perp\rangle, \quad (28)$$

where $|\perp\rangle$ denotes a potentially non-normalized state satisfying $(I_{2^k} \otimes |0\rangle^{\log M} \langle 0|^{\log M}) |\perp\rangle = 0$. Note that the LCU algorithm implements a $(\|\vec{\alpha}\|_1, \log M, 0)$ -block-encoding of $\sum_{j=1}^M \alpha_j U_j$.

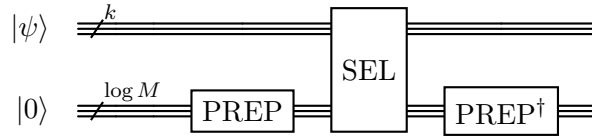


FIGURE 2. Quantum circuit U_{LCU} implementing the LCU algorithm.

3. CLASSICAL ALGORITHM FOR NON-UNIFORM DISCRETE FOURIER TRANSFORM

In this section, we review a classical algorithm for the nonuniform discrete Fourier transform based on a low-rank matrix factorization approach, as presented in [14].

3.1. Type-II NUDFT. We first present the algorithm for the Type-II NUDFT, which assumes uniform frequency points given by $\omega_k = k$ for $k = 0, \dots, N - 1$.

¹A polynomial is said to have parity zero (one) if it is an even (odd) polynomial.

3.1.1. *Perturbed Equispaced Grid Setting.* We begin by describing the algorithm in the special case where the nonuniform grid points are obtained by perturbing an equispaced grid. WLOG, let $\{t_j\}_{j=0}^{N-1} \subseteq [0, 1)$ such that²

$$\left| t_j - \frac{j}{N} \right| \leq \frac{\gamma}{N}, \quad (29)$$

for some $\gamma \in [0, 1/2]$. The simple but important observation is that the entries of F_{II} can be written as

$$(F_{\text{II}})_{jk} = e^{-2\pi i t_j k} = e^{-2\pi i (t_j - \frac{j}{N})k} e^{-2\pi i \frac{jk}{N}}, \quad (30)$$

for $0 \leq j, k \leq N - 1$. This observation leads to the matrix decomposition

$$F_{\text{II}} = A \circ F, \quad (31)$$

where F is the DFT matrix, and the entries of A are given by $A_{jk} = e^{-2\pi i (t_j - j/N)k}$. The matrix A is defined by sampling the bivariate function $(x, y) \mapsto e^{-2\pi i xy}$ over the domain $[-\gamma/N, \gamma/N] \times [0, N]$. As shown in [14], the construction of a low-rank factorization of A is based on approximating this function by a bivariate polynomial of degree $(K - 1)$, which can then be extended to obtain a rank- K approximation of A . This polynomial approximation is derived from a truncated Chebyshev expansion of e^{-ixy} [14, Appendix A]. As a result, the resulting rank- K approximation of A takes the form

$$A_K = \sum_{r=0}^{K-1} \underbrace{\left[\sum_{q=0}^{K-1} \alpha_{qr} \left(\exp(-i\pi N(\vec{t} - \vec{e})) \circ T_p \left(\frac{N(\vec{t} - \vec{e})}{\gamma} \right) \right) \right]}_{\vec{u}_r} T_r \left(\frac{2\vec{\omega}^\top}{N} - \vec{1}^\top \right) \quad (32)$$

$$\begin{cases} 2\vec{v}_r^\top & r = 0 \\ \vec{v}_r^\top & r \geq 1. \end{cases}$$

Here $\vec{e} = (0, \frac{1}{N}, \dots, \frac{N-1}{N})^\top$, $\vec{\omega} = (0, 1, \dots, N - 1)^\top$, and the primes on the summands indicate that the first term should be halved. The coefficients α_{qr} are given by

$$\alpha_{qr} = \begin{cases} 4i^r J_{\frac{q+r}{2}}(-\gamma\pi/2) J_{\frac{r-q}{2}}(-\gamma\pi/2), & \text{if } \text{mod}(|q - r|, 2) = 0, \\ 0, & \text{otherwise} \end{cases} \quad (33)$$

where $J_\nu(\cdot)$ denotes the Bessel function of the first kind of order ν . In order to eliminate the primes in the summand, we define a new quantity α'_{qr} , which will replace α_{qr} in subsequent expressions.

$$\alpha'_{qr} = \begin{cases} \frac{1}{4}\alpha_{qr} & \text{if } q = r = 0, \\ \frac{1}{2}\alpha_{qr} & \text{if } q = 0, r \neq 0 \text{ or } r = 0, q \neq 0, \\ \alpha_{qr} & \text{otherwise} \end{cases} \quad (34)$$

The analysis in [14] shows that it suffices to choose $K = \mathcal{O}\left(\frac{\log(1/\epsilon'_{\text{trunc}})}{\log \log(1/\epsilon'_{\text{trunc}})}\right)$ to ensure that the approximation satisfies $\|A - A_K\|_{\max} \leq \epsilon'_{\text{trunc}}$ for some $\epsilon'_{\text{trunc}} > 0$. Consequently, the matrix F_{II} can then be approximated as

$$F_{\text{II}} = (A \circ F) \approx (A_K \circ F) = \sum_{r=0}^{K-1} D_{\vec{u}_r} F D_{\vec{v}_r}, \quad (35)$$

where $D_{\vec{u}_r} = \text{diag}(\vec{u}_r)$ and $D_{\vec{v}_r} = \text{diag}(\vec{v}_r)$. The last equality follows from the identity $(\vec{u}_r \vec{v}_r^\top) \circ F = D_{\vec{u}_r} F D_{\vec{v}_r}$. Since the complexity of applying F is $\mathcal{O}(N \log N)$, the overall complexity of

²We can compensate for this by introducing a factor of 2π in the complex exponential.

implementing the Type-II NUFFT in the special case where the non-uniform grid points $\{t_j\}_{j=0}^{N-1} \subseteq [0, 1)$ are generated by perturbing an equispaced grid is

$$\mathcal{O}\left(\frac{N \log N \log(1/\epsilon'_{\text{trunc}})}{\log \log(1/\epsilon'_{\text{trunc}})}\right). \quad (36)$$

3.1.2. General Nonuniform Node Distribution. We now discuss how to implement the Type-II NUFFT when the nodes $\{t_j\}_{j=0}^{N-1} \subseteq [0, 1)$ are distributed arbitrarily. The key idea is to reduce the problem to the equispaced case considered previously by identifying a sequence $\{s_j\}_{j=0}^{N-1} \subseteq \{0, \dots, N-1\}$ such that

$$s_j = \begin{cases} m & \text{if } |t_j - \frac{m}{N}| \leq 1/2N \text{ and } m \neq N, \\ 0 & \text{if } |t_j - 1| \leq 1/2N. \end{cases} \quad (37)$$

Note that s_n/N is the closest point to t_j on the equidistant grid $\{0, 1/N, \dots, (N-1)/N\} \subseteq [0, 1)$. We have

$$(F_{\text{II}})_{j,k} = e^{-2\pi i t_j k} = e^{-2\pi i (t_j - \frac{s_j}{N}) k} e^{-2\pi i \frac{s_j k}{N}}. \quad (38)$$

We obtain the matrix decomposition

$$F_{\text{II}} = B \circ F_{\vec{s}}, \quad (39)$$

where $(F_{\vec{s}})_{j,k} = e^{-2\pi i s_j k/N}$, and $B_{jk} = e^{-2\pi i (t_j - s_j/N) k}$. Note that $(F_{\vec{s}})_{j,k}$ is the (k, s_j) -th entry of the DFT matrix, F . As before, the matrix B admits a rank- K approximation via a truncated bivariate Chebyshev approximation applied to each entry. The resulting rank- K approximation of B is then given by

$$B_K = \sum_{r=0}^{K-1} \underbrace{\left[\sum_{q=0}^{K-1} \alpha'_{qr} \left(\exp(-i\pi N(\vec{t} - \vec{s}/N)) \circ T_q(2N(\vec{t} - \vec{s}/N)) \right) \right]}_{\vec{u}_r} \underbrace{\left(\frac{2\vec{\omega}^\top}{N} - \vec{1}^\top \right)}_{\begin{cases} 2\vec{v}_r^\top & r=0 \\ \vec{v}_r^\top & r \geq 1 \end{cases}}. \quad (40)$$

Here $\vec{s} = (s_0, s_1, \dots, s_{N-1})$ and $\vec{\omega} = (0, 1, \dots, N-1)$. The coefficient $\alpha'_{qr} \propto \alpha_{qr}$ in Equation (33) is defined with the choice $\gamma = \frac{1}{2}$. Note that $F_{\vec{s}} = FM_{\vec{s}}$, where

$$(M_{\vec{s}})_{ij} = \begin{cases} 1, & \text{if } i = s_j, \\ 0, & \text{otherwise,} \end{cases} \quad (41)$$

for $0 \leq i, j \leq N-1$. Consequently, F_{II} in the general case can then be approximated as

$$F_{\text{II}} = (B \circ F) \approx (B_K \circ F) = \sum_{r=0}^{K-1} D_{\vec{u}_r} F_{\vec{s}} D_{\vec{v}_r} = \sum_{r=0}^{K-1} D_{\vec{u}_r} F M_{\vec{s}} D_{\vec{v}_r}. \quad (42)$$

Once again, it suffices to choose $K = \mathcal{O}\left(\frac{\log(1/\epsilon'_{\text{trunc}})}{\log \log(1/\epsilon'_{\text{trunc}})}\right)$ to guarantee that $\|B - B_K\|_{\max} \leq \epsilon'_{\text{trunc}}$. The overall computational complexity of the algorithm remains as stated in Equation (36).

3.2. Reduction to Type-II NUFFT. Algorithms for Type-I and Type-III NUFFTs can now be derived from those of the Type-II NUFFT.

(I) **Type-I NUFFT.** The Type-I NUFFT can be efficiently implemented using the Type-II NUFFT. In particular, the entries of the matrix F_{I} satisfy

$$(F_{\text{I}})_{jk} = e^{-2\pi i \frac{j}{N} \omega_k} = e^{-2\pi i \frac{\omega_k}{N} j} = (F_{\text{II}})_{kj}, \quad (43)$$

which shows that F_I is the transpose of F_{II} , where now $\frac{\omega_0}{N}, \dots, \frac{\omega_{N-1}}{N}$ assume the role of non-equispaced sample points in a Type-I NUQFT. Hence, F_I can be approximated as

$$F_I = F_{II}^T \approx \sum_{r=0}^{K-1} (D_{\vec{u}_r} F M_{\vec{s}} D_{\vec{v}_r})^T = \sum_{r=0}^{K-1} D_{\vec{v}_r} M_{\vec{s}}^T F^T D_{\vec{u}_r}. \quad (44)$$

Note that F^T can be efficiently computed using the inverse FFT. Therefore, the Type-I NUQFT may be realized via the Type-II NUQFT, inheriting the same computational complexity.

- (III) **Type-III NUQFT.** The Type-III NUQFT can be also efficiently implemented using the Type-II NUQFT. It is shown in [14] the entries of the matrix F_{III} satisfy

$$(F_{III}) = A \circ B \circ (F M_{\vec{s}}) := A \circ B \circ (F_I)_{\vec{s}}, \quad (45)$$

where $A_{jk} = e^{-2\pi i(t_j - s_j/N)\omega_k}$, B is a matrix of rank at most 2 and $(F_I)_{\vec{s}}$ is obtained extracting the columns indexed by (s_0, \dots, s_{N-1}) from F_I . Therefore, the Type-III NUQFT may be realized via the Type-II NUQFT, inheriting the same computational complexity.

4. QUANTUM ALGORITHM FOR NON-UNIFORM DISCRETE FOURIER TRANSFORM

We now present a quantum algorithm for the Non-Uniform Quantum Fourier Transform (NUQFT) based on the low-rank factorization framework reviewed in Section 3. Throughout, we assume that $N = 2^n$ for some $n \geq 1$ and restrict attention to the Type-II NUQFT. The overall approach may be summarized as follows:

- (1) **Construction of $U_{\vec{v}_r}$.** We first construct quantum circuits that encode the coefficient vectors \vec{v}_r , defined as follows:

$$(\vec{v}_r)_j = \begin{cases} 2^{-1} T_0(2j/N - 1), & r = 0, \\ T_r(2j/N - 1), & r \geq 1. \end{cases} \quad (46)$$

For each r , we construct a unitary operator $U_{\vec{v}_r}$ that encodes the entries of \vec{v}_r as amplitudes of a quantum state.

- (2) **Construction of $U_{\vec{u}_r}$.** We next construct quantum circuits that encode the coefficient vectors \vec{u}_r , defined as follows:

$$(\vec{u}_r)_j = \sum_{q=0}^{K-1} \alpha'_{qr} e^{-i\pi N(t_j - s_j/N)} T_q(2N(t_j - s_j/N)). \quad (47)$$

For each r , we construct a unitary operator $U_{\vec{u}_r}$ that encodes the entries of \vec{u}_r as amplitudes of a quantum state.

- (3) **Block-encoding Operators.** Using $U_{\vec{v}_r}$ and $U_{\vec{u}_r}$, we implement block encodings of the diagonal matrices $D_{\vec{v}_r}$ and $D_{\vec{u}_r}$. These are combined with a standard block encoding of the Fourier transform and the matrix $M_{\vec{s}}$ defined in Equation (41).
- (4) **Assembly via LCU.** Finally, we employ the Linear Combination of Unitaries (LCU) algorithm to combine the block-encoded matrix products, thereby implementing a block encoding of the Type-II non-uniform discrete Fourier transform.

Remark 8. In what follows, a quantum register denotes a collection of qubits prepared in superposition over computational basis states. Ancilla qubits serve as auxiliary qubits for intermediate operations within a circuit, while a computational qubit is the qubit in which the final result is stored. Any deviation from this convention will be stated explicitly.

4.1. **Construction of $U_{\vec{v}_r}$.** We first construct $U_{\vec{v}_r}$. The case $r = 0$ is particularly simple, since $(\vec{v}_0)_{j,j} = \frac{1}{2}$ because $T_0(x) \equiv 1$. We prepare a quantum register encoding j in uniform superposition, together with an ancilla qubit whose $|0\rangle$ amplitude represents the constant value $\frac{1}{2}$ for all j in the superposition. The corresponding quantum circuit, denoted $U_{\vec{v}_0}$, can be implemented directly.

Proposition 9. *Let $n \in \mathbb{N}$. The unitary operator $U_{\vec{v}_0}$ can be implemented using $\mathcal{O}(n)$ Hadamard gates and $\mathcal{O}(1)$ single-qubit rotation gates.*

Proof. Prepare an n -qubit register in uniform superposition over all computational basis states using n Hadamard gates. Next, prepare a single computational qubit in the state $\frac{1}{2}|0\rangle + \frac{i\sqrt{3}}{2}|1\rangle$ using a single-qubit rotation of the form $e^{i\pi/3\sigma_X}$. This defines the unitary $U_{\vec{v}_0}$. The corresponding pseudocode is given in Algorithm 2. \square

Algorithm 2: Preparation of $U_{\vec{v}_0}$

Input: Integer $n \geq 1$

Output: Quantum state with $U_{\vec{v}_0}$ applied in superposition

Initialize $(n + 1)$ qubits $|0\rangle|0\rangle^n$

for $i \leftarrow 2$ **to** $n + 1$ **do**

 Apply Hadamard gate H to qubit i in $|0\rangle^n$

 Apply single-qubit rotation $e^{i\pi/3\sigma_X}$ to the computational qubit

return Quantum state $U_{\vec{v}_0}|0\rangle|0\rangle^n = \frac{1}{\sqrt{2^n}} \sum_j (\frac{1}{2}|0\rangle + \frac{i\sqrt{3}}{2}|1\rangle)|j\rangle$

Before proceeding, we first prove a lemma on how to compute $1 - x$ on a quantum computer, where $x \in (0, 1)$.

Lemma 10. *Let $k \in \mathbb{N}$ and let $x \in (0, 1)$ be stored in binary in a k -qubit computational register. There exists a quantum circuit U_{neg} acting on the k -qubit register such that $U_{\text{neg}}|x\rangle = |1 - x\rangle$. Moreover, U_{neg} can be implemented using $\mathcal{O}(k)$ σ_X gates, $\mathcal{O}(k)$ CNOT gates, and $\mathcal{O}(k)$ Toffoli gates.*

Proof. Let $x = 0.x_1x_2\dots x_k$ be a k -bit fractional number expressed in binary, so that $x = \sum_{i=1}^k x_i 2^{-i}$. We define the bitwise complement of x as $\bar{x} = 0.\bar{x}_1\bar{x}_2\dots\bar{x}_k$, where $\bar{x}_i = 1 - x_i$ for each $i = 1, \dots, k$. Then

$$\bar{x} = \sum_{i=1}^k \bar{x}_i \cdot 2^{-i} = \sum_{i=1}^k (1 - x_i) 2^{-i} = \sum_{i=1}^k 2^{-i} - \sum_{i=1}^k x_i 2^{-i} = 1 - 2^{-k} - \sum_{i=1}^k x_i 2^{-i} = 1 - x - 2^{-k}. \quad (48)$$

\bar{x} can be computed by applying the σ_X gate to each of the k qubits. It remains to add 2^{-k} . This is a standard application of binary arithmetic and can be implemented by invoking the oracle U_{AM} using $\mathcal{O}(k)$ CNOT and Toffoli gates. The resulting quantum circuit is denoted by U_{neg} . \square

We now construct $U_{\vec{v}_r}$ for $r \geq 1$. In Proposition 11, a parameter $p \in \mathbb{N}$ is selected to facilitate the approximation of $\arccos(\cdot)$ on a quantum computer to arbitrary precision. This parameter is chosen freely at this stage, and will be fixed to a specific value later when required.

Proposition 11. *Let $p, r, n \in \mathbb{N}$. $U_{\vec{v}_r}$ can be implemented using $\mathcal{O}(n)$ Hadamard gates, $\mathcal{O}(n + p^2)$ CNOT gates, $\mathcal{O}(n)$ σ_X gates and $\mathcal{O}(p)$ single-qubit controlled rotation gates generated by σ_X . The corresponding quantum circuit has depth $\mathcal{O}(p \log p)$.*

Proof. Initialize two quantum registers of n qubits, $\mathcal{O}(p)$ ancilla qubits, and one computational qubit, all initialized to $|0\rangle$. We index the first quantum register of n qubits from 0 to $n - 1$. Apply Hadamard gates to the first quantum register to construct the state $\frac{1}{\sqrt{2^n}} \sum_{j=0}^{2^n-1} |0\rangle|j\rangle|0\rangle^n|0\rangle^p$. Let

$$x_j := \frac{2j}{N} - 1 = \frac{\sum_{k=0}^{n-1} j_k 2^k}{2^{n-1}} - 1 = \sum_{k=0}^{n-1} j_k 2^{k-n+1} - 1 = \sum_{k=0}^{n-2} j_k 2^{k-(n-1)} + j_{n-1} - 1 \in [-1, 1). \quad (49)$$

We first represent x_j in a fixed-point binary format. In what follows, we index the qubits in the second quantum register from 1 to n . The construction proceeds as follows:

- (1) For $k = 0$ to $n - 2$, apply a CNOT gate with the control on the k -th qubit of the first quantum register and the target on the m -th qubit of the second quantum register, where $m + k = n - 1$. This step ensures that the first $n - 1$ qubits in the second quantum register encode the fraction $\sum_{k=0}^{n-2} j_k 2^{k-n+1}$.
- (2) If $j_{n-1} = 1$, the construction is complete. If $j_{n-1} = 0$, then we must compute $\sum_{k=0}^{n-2} j_k 2^{k-n+1} - 1 \in [-1, 0)$. This is achieved by applying a controlled unitary operator, with the control on the last qubit of the first quantum register and the target on the second quantum register. The operator acts only if the control qubit is in the state $|0\rangle$. The sign is stored in the last qubit of the second quantum register, with $|1\rangle$ denoting a negative sign, while the first $n - 1$ qubits encode the absolute value

$$\left| \sum_{k=0}^{n-2} j_k 2^{k-(n-1)} - 1 \right| = 1 - \sum_{k=0}^{n-2} j_k 2^{k-(n-1)}. \quad (50)$$

This can be implemented using Lemma 10.

We now construct the entry $(\vec{v}_r)_j$ in superposition using the quantum signal processing (QSP) algorithm. We implement $e^{ir \arccos(x_j)\sigma_X}$. This requires computing $\theta_j = \arccos(x_j)$, which can be obtained by first computing $\arcsin(x_j)$ using the algorithm of Burge et al. [51] as in Section 2.3.1, and then applying $\arccos(x_j) = \pi/2 - \arcsin(x_j)$. Using the p ancilla qubits to store the approximation $\widehat{\theta}_j = \widehat{\arccos}(x_j)$ ³, we have

$$|\widehat{\theta}_j - \theta_j| \leq 2^{-p+1}. \quad (51)$$

We label this unitary operator U_{\arccos} , which can be implemented using $\mathcal{O}(p^2)$ CNOT gates and a circuit of depth $\mathcal{O}(p \log p)$. Note that we can write

$$\widehat{\theta}_j = b_1^{(\theta_j)} 2^1 + b_0^{(\theta_j)} 2^0 + \sum_{k=-1}^{-(p-2)} b_k^{(\theta_j)} 2^k := \sum_{k=1}^{-(p-2)} b_k^{(\theta_j)} 2^k, \quad b_k^{(\theta_j)} \in \{0, 1\}, \quad (52)$$

since $\theta \in [0, \pi]$. We can implement $e^{ir \widehat{\theta}_j \sigma_X} := R_X(-r \widehat{\theta}_j)$ via the following formula:

$$R_X(-r \widehat{\theta}_j) = R_X \left(-r \sum_{k=1}^{-(p-2)} b_k^{(\theta_j)} 2^k \right) = \prod_{k=1}^{-(p-2)} R_X(-r 2^k)^{b_k^{(\theta_j)}}. \quad (53)$$

If we adopt the convention of numbering the qubits in the p -qubit register from 1 down to $-(p-2)$, we have

$$R_X(-r \widehat{\theta}_j) = \prod_{k=1}^{-(p-2)} \left(|0\rangle\langle 0|_k \otimes I + |1\rangle\langle 1|_k \otimes R_X(-r 2^k) \right). \quad (54)$$

This step requires $\mathcal{O}(p)$ applications of single-qubit controlled rotation gates generated by σ_X . Using [52, Equation (45)], which provides the explicit expression for $e^{ir \arccos(x)\sigma_X}$, the resulting quantum state is given by

$$U_{\vec{v}_r} |0\rangle |0\rangle^{2n} |0\rangle^p = \frac{1}{\sqrt{2^n}} \sum_{j=0}^{2^n-1} \left(T_r(x_j) |0\rangle + i\sqrt{1-x_j^2} S_{r-1}(x_j) |1\rangle \right) |j\rangle |x_j\rangle^n |\widehat{\arccos}(x_j)\rangle^p. \quad (55)$$

Here we have used that $T_r(x) = \cos(r \arccos(x))$. See Algorithm 3 and Figure 3 for the corresponding pseudocode and quantum circuit. \square

³The p -bit binary representation of $\pi/2$ can be computed classically and used to obtain a p -bit approximation of $\pi/2 - \arcsin(x_j)$ in the p -qubit register containing $\widehat{\theta}_j = \widehat{\arcsin}(x_j)$. Since this operation does not change the overall circuit complexity, we assume that it is incorporated within the quantum circuit, U_{\arccos} .

Algorithm 3: Construction of $U_{\vec{v}_r}$ for $r \geq 1$

Input: $p, n, r \in \mathbb{N}$ and U_{neg} from Lemma 10

Output: Quantum state with $U_{\vec{v}_r}$ applied in superposition

Initialize $1 + 2n + p$ qubits to $|0\rangle$

Apply Hadamard gates to first register of n qubits

for $k \leftarrow 0$ **to** $n - 2$ **do**

└ Apply CNOT with control k in 1st register and target $m = n - k - 1$ in 2nd register

Apply $C-U_{\text{neg}}$ with control last qubit of 1st register and target first $n - 1$ qubits on 2nd register

Apply CNOT with control last qubit of 1st register and target last qubit on 2nd register

Compute (an approximation to) $\theta_j = \arccos(x_j)$ using U_{\arccos} on p -qubit ancilla

for $k \leftarrow 1$ **down to** $-(p - 2)$ **do**

└ **if** $b_k^{(\theta_j)} = 1$ in θ_j register **then**

└└ Apply controlled rotation $e^{ir2^k\sigma_x}$ with control on ancilla qubit k
return Quantum state $U_{\vec{v}_r} |0\rangle |0\rangle^{2n} |0\rangle^p$

The second quantum register of n qubits, together with the p ancilla qubits, can be uncomputed, yielding a unitary $U'_{\vec{v}_r}$ such that

$$U'_{\vec{v}_r} |0\rangle |0\rangle^{2n} |0\rangle^p = \frac{1}{\sqrt{2^n}} \sum_{j=0}^{2^n-1} \left(T_r(x_j) |0\rangle + i\sqrt{1-x_j^2} U_{r-1}(x_j) |1\rangle \right) |j\rangle |0\rangle^n |0\rangle^p. \quad (56)$$

This step does not alter the computational complexity of the quantum circuit. For notational simplicity, we continue to denote $U'_{\vec{v}_r}$ by $U_{\vec{v}_r}$.

4.2. Construction of $U_{\vec{u}_r}$. We now construct $U_{\vec{u}_r}$. The expression for $(\vec{u}_r)_j$ is determined by $\vec{t} \in [0, 1]^{2^n}$. Since \vec{t} is arbitrary, we assume access to the following oracle as part of the algorithm.

Assumption 12. For $m \geq n$, we assume access to the oracle $O_{\vec{t}}^{(m)}$ such that

$$O_{\vec{t}}^{(m)} : |i\rangle |0\rangle^m \mapsto |i\rangle |t_i^{(m)}\rangle^m = \bigotimes_{j=1}^m |i\rangle |t_i^{(j)}\rangle, \quad (57)$$

where $t_i^{(m)} = \sum_{j=1}^m t_i^{(j)} 2^{-j} = 0.t_i^{(1)} \dots t_i^{(m)}$ is the m -bit binary representation of t_i . The parameter m is left arbitrary for now and will be fixed to a specific value as required.

Remark 13. In practice, such oracles correspond to data structures that allow efficient superposition queries to classical datasets (e.g., QRAM). While building these structures efficiently remains an active research topic, this assumption is standard in the design of quantum linear-algebra algorithms.

The first step is to compute $\vec{s} = (s_0, s_1, \dots, s_{2^n-1})$, as defined in Equation (37). The vector \vec{s} can be computed as

$$s_i = \begin{cases} \text{round}(Nt_i) & \text{if } \text{round}(Nt_i) < N \\ 0 & \text{if } \text{round}(Nt_i) = N, \end{cases} \quad (58)$$

where $N = 2^n$ and $\text{round}(\cdot)$ denotes rounding to the nearest integer. In fact, we now explicitly construct a quantum circuit that implements the oracle

$$O_{\vec{s}}^{(m)} : |i\rangle |0\rangle^m \mapsto |i\rangle |s_i^{(m)}\rangle^m = \bigotimes_{j=1}^m |i\rangle |s_i^{(j)}\rangle, \quad (59)$$

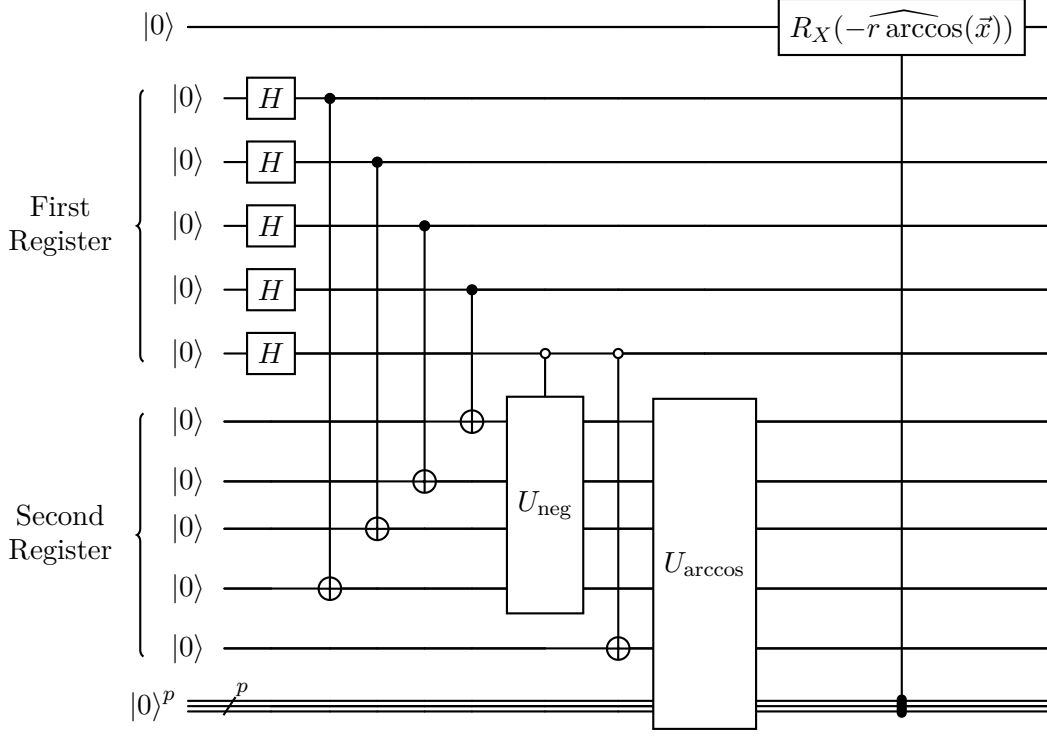


FIGURE 3. Quantum circuit implementing $U_{\vec{v}_r}$ for $r \geq 1$ in the special case $n = 5$.

where $s_i^{(m)}$ is the m -bit representation of s_i/N . We first claim that the operation $N\vec{t}$ can be implemented efficiently.

Lemma 14. *Let $n \in \mathbb{N}, m \geq n$ and $\vec{t} \in [0, 1]^{2^n}$. $N\vec{t}$ can be computed using $\mathcal{O}(1)$ queries to $O_{\vec{t}}^{(m)}$ and $\mathcal{O}(n)$ Hadamard gates on an $\mathcal{O}(n+m)$ qubit circuit.*

Proof. Initialize an $(n+m)$ -qubit quantum register in $|0\rangle$. Apply Hadamard gates to the first n qubits to prepare the uniform index superposition $\frac{1}{\sqrt{2^n}} \sum_{i=0}^{2^n-1} |i\rangle |0\rangle^m$. Querying $O_{\vec{t}}^{(m)}$ yields

$$O_{\vec{t}}^{(m)} |0\rangle^{n+m} = \frac{1}{\sqrt{2^n}} \sum_{i=0}^{2^n-1} \bigotimes_{j=1}^m |t_i^{(j)}\rangle. \quad (60)$$

Multiplication by N yields $Nt_i^{(m)} = t_i^{(1)} \cdots t_i^{(n)} \cdot t_i^{(n+1)} \cdots t_i^{(m)}$, where the first n bits correspond to $\lfloor Nt_i \rfloor$, and the remaining $m-n$ bits correspond to the fractional part. No additional quantum gates are required. \square

The next step is to round each Nt_i to the nearest integer, a nontrivial operation only when $\lfloor t_i^{(n+1)} \rfloor = 1$. This rounding can be implemented as a controlled unitary, denoted U_{round} . In this setting, rounding the binary string $t_i^{(1)} \cdots t_i^{(n)}$ amounts to computing the binary sum $t_i^{(1)} \cdots t_i^{(n)} \oplus 1$. Equivalently, this corresponds to the map $|x\rangle \mapsto |x \oplus y\rangle$, where $|x\rangle = |t_i^{(1)} \cdots t_i^{(n)}\rangle$ and $|y\rangle = |t_i^{(n+1)}\rangle$. This operation can be realized using the oracle U_{AM} .

Proposition 15. *Let $n \in \mathbb{N}$ and $m \geq n$. The oracle $O_{\vec{s}}^{(m)}$ can be implemented using a $\mathcal{O}(n+m)$ -qubit quantum circuit, $\mathcal{O}(1)$ queries to the oracle $O_{\vec{t}}^{(m)}$, $\mathcal{O}(n)$ Hadamard gates and $\mathcal{O}(m)$ Toffoli, CNOT and σ_X gates.*

Proof. This follows directly from Lemma 14 together with the use of U_{AM} , noting that the m -bit representation of s_i/N is stored in the m -qubit register upon application of circuit in Figure 4. \square

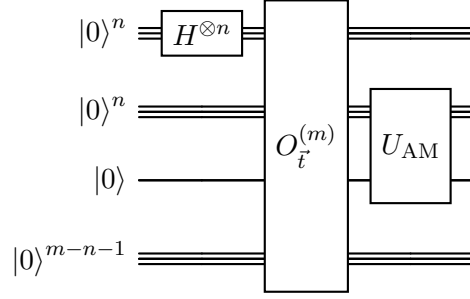


FIGURE 4. Quantum circuit implementing $O_s^{(m)}$.

Having constructed the oracle $O_s^{(m)}$, the next step is to construct $U_{\vec{u}_r}$ for $r \geq 0$, which implements $(\vec{u}_r)_j$. We first establish a lemma analogous to Lemma 10, which enables the computation of $x - y$ for $x, y \in [0, 1)$ using the quantum circuit U_{subtract} .

Remark 16. In what follows, when we state that a quantum register is “multiplied by 2^k ” for some $k \geq 1$, we mean a reinterpretation of the same qubit register under a fixed-point encoding in which the binary point is shifted k positions to the right. No quantum gates are applied; this is purely a change in the numerical interpretation of the register contents. Similarly, “division by 2^k ” corresponds to shifting the binary point k positions to the left.

Lemma 17. *Let $m \in \mathbb{N}$ and let $x, y \in [0, 1)$ be stored in k -qubit registers. There exists a unitary operator U_{subtract} that computes the signed difference $x - y \in (-1, 1)$ using $\mathcal{O}(k)$ CNOT, Toffoli, and σ_X gates.*

Proof. Let $x = 0.x_1x_2\dots x_k$ and $y = 0.y_1y_2\dots y_k$ be the k -bit fractional binary representations of x and y , so that $x = \sum_{i=1}^k x_i 2^{-i}$ and $y = \sum_{i=1}^k y_i 2^{-i}$. Multiply x and y by 2^k to obtain integers

$$X = \sum_{i=1}^k x_i 2^{k-i} = x \cdot 2^k, \quad Y = \sum_{i=1}^k y_i 2^{k-i} = y \cdot 2^k. \quad (61)$$

Note that $X, Y \in \{0, 1, \dots, 2^k - 1\}$. Embed X and Y into $(k + 1)$ -qubit registers by adding a leading sign bit set to 0, thereby interpreting them as signed integers. We have

$$X = 0 \cdot 2^k + \sum_{i=1}^k x_i 2^{k-i}, \quad Y = 0 \cdot 2^k + \sum_{i=1}^k y_i 2^{k-i}. \quad (62)$$

Compute the bitwise complement of Y :

$$\bar{Y} = 1 \cdot 2^k + \sum_{i=1}^k \bar{y}_i 2^{k-i} = 1 \cdot 2^k + \sum_{i=1}^k (1 - y_i) 2^{k-i} = 1 \cdot 2^k + \sum_{i=1}^k 2^{k-i} - \sum_{i=1}^k y_i 2^{k-i} = 2^{k+1} - Y - 1. \quad (63)$$

\bar{Y} is obtained by applying a σ_X gate to each of the $k + 1$ qubits encoding Y . Adding 1 yields $-Y := \bar{Y} + 1 = 2^{k+1} - Y$, ignoring overflow. In binary arithmetic, $\bar{Y} + 1$ is the two’s complement of Y and represents its negative when the $(k + 1)$ -st qubit serves as the sign bit.⁴ This justifies the notation $-Y$. Applying U_{AM} to compute $X + (-Y)$ produces the signed integer $Z = X - Y$. Interpreting Z as a fixed-point number by dividing by 2^k gives $\frac{Z}{2^k} = x - y \in (-1, 1)$. Since $x, y \in [0, 1)$, no overflow occurs. The circuit requires $\mathcal{O}(k)$ CNOT, Toffoli, and σ_X gates. \square

⁴The identity $-Y := \bar{Y} + 1$ is the standard two’s complement representation.

Algorithm 4: Computation of $x - y$ using signed fixed-point arithmetic (U_{subtract})

Input: k -qubit registers $|x\rangle = |x_1 \cdots x_k\rangle$ and $|y\rangle = |y_1 \cdots y_k\rangle$ encoding $x, y \in [0, 1)$
Output: $(k + 1)$ -qubit register encoding the signed fixed-point value $x - y$
Scale $|x\rangle$ and $|y\rangle$ by 2^k to obtain integer registers $|X\rangle$ and $|Y\rangle$
Append a leading qubit $|0\rangle$ to each register to form signed $(k + 1)$ -qubit registers
for $i \leftarrow 1$ **to** $k + 1$ **do**
 | Apply σ_X to qubit i of $|Y\rangle$
Add 1 to $|Y\rangle$ to obtain the two's-complement encoding of $-Y$
Compute $|X - Y\rangle$ using U_{AM}
Interpret the result as a signed fixed-point number by dividing by 2^k
return Computational register representing $|x - y\rangle$

We construct $U_{\vec{u}_r}$ for $r \geq 0$ by first computing $\vec{t} - \vec{s}/N$ using the preceding routines, and then implementing $T_q(2N(\vec{t} - \vec{s}/N))$ via quantum signal processing (QSP). Complex exponential factors are realized through σ_Z -generated rotations, and the weighted Chebyshev terms are combined using the linear combination of unitaries (LCU) technique. We further assume access to a suitable state-preparation oracle.

Assumption 18. We assume access to a state-preparation oracle

$$\text{PREP}_r |0\rangle = \frac{1}{\sqrt{\|\vec{\alpha}'_r\|_1}} \sum_{q=0}^{K-1} \sqrt{\alpha'_{qr}} |q\rangle, \quad (64)$$

where α'_{qr} are defined in Equation (33) and Equation (34) with $\gamma = 1/2$.

Proposition 19. Let $m, p, K \in \mathbb{N}$ and $r \in \mathbb{N} \cup \{0\}$. $U_{\vec{u}_r}$ can be implemented using $\mathcal{O}(m + n + p + \log K)$ qubits, $\mathcal{O}(1)$ queries to $O_{\vec{t}}^{(m)}$, $\mathcal{O}(n)$ Hadamard gates, $\mathcal{O}(m + p^2)$ CNOT gates, $\mathcal{O}(m)$ Toffoli gates, $\mathcal{O}(m)$ σ_X gates, and $\mathcal{O}(p + m)$ single-qubit controlled rotation gates. The corresponding quantum circuit has depth $\mathcal{O}(m + p \log p + \log K)$.

Proof. Consider a $(1 + n + 2m + \mathcal{O}(p))$ -qubit system, with all qubits initialized to $|0\rangle$. First, apply Hadamard gates to the quantum register of n qubits, and then apply the oracles $O_{\vec{t}}^{(m)}$ and $O_{\vec{s}}^{(m)}$ on the two m -qubit ancilla registers to construct the state

$$\frac{1}{\sqrt{2^n}} \sum_{i=0}^{2^n-1} |0\rangle |i\rangle |t_i^{(m)}\rangle^m |s_i^{(m)}/N\rangle^m |0\rangle^p. \quad (65)$$

Invoking Lemma 17, we compute $\vec{t} - \vec{s}/N$ in superposition within the quantum register containing \vec{s}/N .⁵ We then compute an approximation of $\arccos(2N(\vec{t} - \vec{s}/N))$. The multiplication by $2N$ is implemented reversibly as a constant-factor scaling on the fixed-point representation of $\vec{t} - \vec{s}/N$. Since $2N$ is a power of two, this operation reduces to a bit shift and therefore does not affect the overall complexity of the quantum circuit. By invoking U_{\arccos} as in Proposition 11, we obtain an approximation of $\arccos(2N(\vec{t} - \vec{s}/N))$ in superposition within the p -qubit register. We denote the quantum circuit implementing this scaling step followed by U_{\arccos} by U'_{\arccos} . As in Proposition 11, we implement a controlled rotation $R_X(-q \arccos(2N(\vec{t} - \vec{s}/N)))$ to realize the Chebyshev polynomial $T_q(x)$. Similarly, we implement a controlled rotation $R_Z(\pi N(\vec{t} - \vec{s}/N))$ to realize the phase factor $e^{-i\pi N(\vec{t} - \vec{s}/N)}$. Denote the unitary operator constructed above by U_q . Finally, using the state-preparation oracle in Equation (64), we apply the LCU algorithm to implement the desired expression via the operator $U_{\vec{u}_r} = \sum_{q=0}^{K-1} \alpha'_{qr} U_q$. We need to append an $\mathcal{O}(\log K)$ ancilla

⁵A single ancilla qubit can be appended to encode the sign of $t_j - s_j/N$ without affecting the overall complexity. This ancilla qubit is used in Lemma 17.

Algorithm 5: Implementation of $U_{\vec{u}_r}$

Input: Integers $n, m, p \geq 1$, system size $n + 2m + p + 1$ qubits
Output: Operator $U_{\vec{u}_r} = \sum_{q=0}^{K-1} \alpha'_{qr} U_q$ applied in superposition
Initialize all $n + 2m + p + 1$ qubits to $|0\rangle$
Apply Hadamard gates $H^{\otimes n}$ to the n -qubit register
Apply oracles $O_{\vec{t}}^{(m)}$ and $O_{\vec{s}}^{(m)}$ to the two m -qubit registers
Compute $\vec{t} - \vec{s}/N$ in the \vec{t} -register using U_{subtract} (see Algorithm 4)
Apply U_{arccos} to approximate $\arccos(\vec{t} - \vec{s}/N)$ in the p -qubit register
Apply controlled rotation $R_X(-q \arccos(2N(\vec{t} - \vec{s}/N)))$ to realize $T_q(x)$
Apply controlled rotation $R_Z(\pi N(\vec{t} - \vec{s}/N))$ to realize $e^{-i\pi N(\vec{t} - \vec{s}/N)}$
Append $\mathcal{O}(\log K)$ ancilla qubits
Denote the resulting unitary as U_q
Use LCU method to implement $U_{\vec{u}_r} = \sum_{q=0}^{K-1} \alpha'_{qr} U_q$ via U_{LCU}
return $U_{\vec{u}_r} |0\rangle^{(n+2m+p+1+\mathcal{O}(\log K))}$

qubits to invoke the LCU algorithm. The complexity estimates follow from previous complexity estimates and the observation that a $\mathcal{O}(\log K)$ -qubit controlled gate acting can be implemented via a quantum circuit using only CNOT gates and single-qubit gates such that the circuit has depth $\mathcal{O}(\log K)$ [55]. If $y_i^{(m)} = t_i^{(m)} - s_i^{(m)}/N$, the resulting quantum state $U_{\vec{u}_r} |0\rangle^{(n+2m+p+1+\mathcal{O}(\log K))}$ is given by

$$\frac{1}{\sqrt{2^n}} \sum_{i=0}^{2^n-1} \left(\frac{1}{\|\vec{\alpha}'_r\|_1} \left(\sum_{q=0}^{K-1} \alpha'_{qr} U_q |0\rangle \right) |0\rangle^{\mathcal{O}(\log K)} + |\perp\rangle \right) |i\rangle |t_i^{(m)}\rangle^m |y_i^{(m)}\rangle^m |\widehat{\arccos}(y_i^{(m)})\rangle^p, \quad (66)$$

where $|\perp\rangle$ is a state that is orthogonal to $(\sum_{q=0}^{K-1} \alpha'_{qr} U_q |0\rangle) |0\rangle^{\mathcal{O}(\log K)}$. See Figure 5 for the corresponding quantum circuit and Algorithm 5 for the corresponding pseudocode. \square

Once again, the ancilla qubits can be uncomputed, yielding a unitary $U'_{\vec{u}_r}$ such that the output quantum state is

$$\frac{1}{\sqrt{2^n}} \sum_{i=0}^{2^n-1} \left(\frac{1}{\|\vec{\alpha}'_r\|_1} \left(\sum_{q=0}^{K-1} \alpha'_{qr} U_q |0\rangle \right) |0\rangle^{\mathcal{O}(\log K)} + |\perp\rangle \right) |i\rangle |0\rangle^{2m} |0\rangle^p. \quad (67)$$

This step does not change the computational complexity of the quantum circuit. For notational simplicity, we continue to denote $U'_{\vec{u}_r}$ by $U_{\vec{v}_r}$. Note that, in Figure 5, we have departed from the usual convention of placing the ancilla qubits $|0\rangle^{\mathcal{O}(\log K)}$ below the n -qubit register. This deviation was necessary to avoid awkward placement of the U_{LCU} gate in the circuit diagram.

4.3. Block Encoding Operators. We now use $U_{\vec{u}_r}$ and $U_{\vec{v}_r}$ within a block-encoding framework to implement the diagonal matrices $D_{\vec{u}_r}$ and $D_{\vec{v}_r}$. We assume that the ancilla qubits used to implement $U_{\vec{v}_r}$ and $U_{\vec{u}_r}$ have been uncomputed, as discussed above. These qubits will not be referenced in any equations or quantum circuits below; however, their usage is accounted for in the overall complexity analysis of the algorithm in Theorem 24. Recall that $U_{\vec{v}_r}$ acts on $|j\rangle |0\rangle$ as

$$U_{\vec{v}_r} |j\rangle |0\rangle = |j\rangle (v_r(j) |0\rangle + \sqrt{1 - v_r(j)^2} |1\rangle). \quad (68)$$

The top-left block of $U_{\vec{v}_r}$ corresponds exactly to the desired diagonal matrix:

$$(|0\rangle \otimes I) U_{\vec{v}_r} (|0\rangle \otimes I) = D_{\vec{v}_r}. \quad (69)$$

This yields a $(1, 1, 0)$ block encoding of $D_{\vec{v}_r}$.

Example 20. Let $N = 4$, so that $D_{\vec{v}_r} = \text{diag}(v_r(0), v_r(1), v_r(2), v_r(3))$. We abbreviate $i\sqrt{1 - v_r(0)^2}$ as $v'_r(0)$. After uncomputing and ignoring any auxiliary registers, the matrix representation of $U_{\vec{v}_r}$ block encodes $D_{\vec{v}_r}$ as follows:

$$U_{\vec{v}_r} = \left(\begin{array}{cccc|cccc} v_r(0) & & & & * & & & \\ & v_r(1) & & & & * & & \\ & & v_r(2) & & & & * & \\ & & & v_r(3) & & & & * \\ \hline v'_r(0) & & & & * & & & \\ & v'_r(1) & & & & * & & \\ & & v'_r(2) & & & & * & \\ & & & v'_r(3) & & & & * \end{array} \right) \quad (70)$$

We have adopted the basis convention $\{|000\rangle, |010\rangle, |100\rangle, |110\rangle, |001\rangle, |011\rangle, |101\rangle, |111\rangle\}$ in the matrix representation of $U_{\vec{v}_r}$ above, where the first qubit corresponds to the computational qubit. Projecting onto the computational state $|0\rangle$ extracts the top-left submatrix:

$$(\langle 0| \otimes I_4) U_{\vec{v}_r} (|0\rangle \otimes I_4) = \begin{pmatrix} v_r(0) & & & \\ & v_r(1) & & \\ & & v_r(2) & \\ & & & v_r(3) \end{pmatrix} = D_{\vec{v}_r}. \quad (71)$$

A similar argument yields a block encoding of $D_{\vec{u}_r}$. The only difference is that $D_{\vec{u}_r} / \|\vec{\alpha}'_r\|_1$ is block encoded, since \vec{u}_r is implemented via the LCU method. Consequently, we obtain a $(\|\vec{\alpha}'_r\|_1, 1, 0)$ block encoding of $D_{\vec{u}_r}$. Furthermore, recall that $F_{\vec{s}} = FM_{\vec{s}}$, where $M_{\vec{s}}$ is defined in Equation (41). Since F is unitary, a block encoding of F is immediate. Since $M_{\vec{s}}$ is a binary (0–1) matrix, we can apply Lemma 5 to obtain a block encoding of $M_{\vec{s}}$. Observe that $M_{\vec{s}}$ is a 1-column-sparse matrix and that the oracle $O_{\vec{s}}^{(m)}$ effectively realizes the column-access oracle O_c . In this setting, it suffices to choose $m = n$. We further note that the row-access oracle O_r corresponds to access to the inverse mapping of $\vec{t} \mapsto \vec{s}$. For generic \vec{t} and \vec{s} , constructing O_r from $O_{\vec{t}}$ and $O_{\vec{s}}$ may require additional pre-processing or data-structure assumptions; accordingly, we treat O_r as an independent primitive.

Assumption 21. We assume black-box access to the row-access oracle O_r required by Lemma 5.

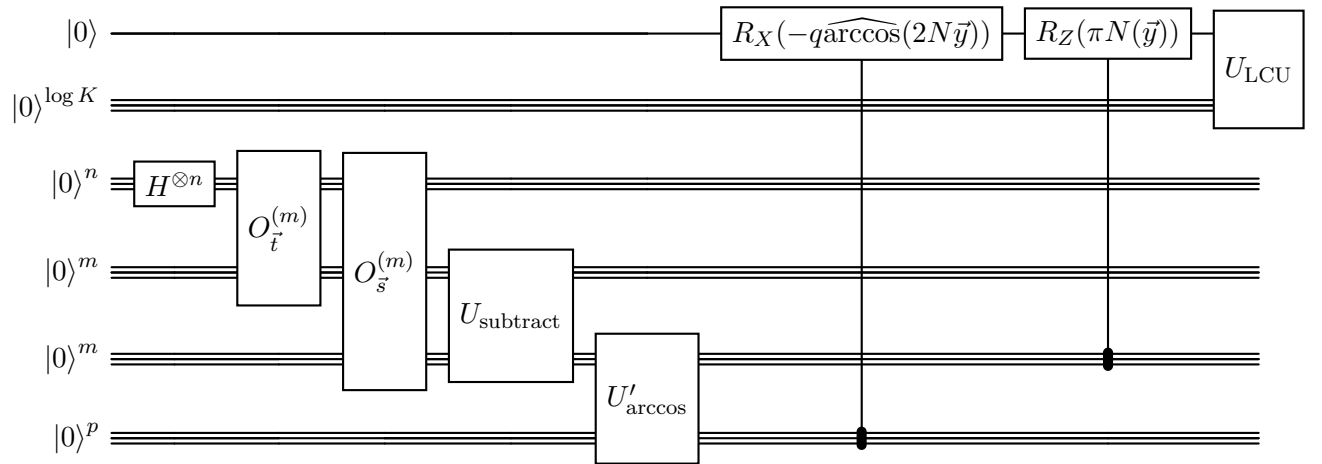


FIGURE 5. Quantum circuit implementing the operator $U_{\vec{u}_r} = \sum_{q=0}^{K-1} \alpha'_{qr} U_q$. We have abbreviated $\vec{t} - \vec{s}/N$ by \vec{y} .

The oracle O_A can be implemented efficiently. Specifically, we construct O_A by appending an additional n -qubit register and applying $O_s^{(n)}$ to obtain

$$|0\rangle^n |i\rangle |j\rangle |0\rangle \mapsto |s_j\rangle |i\rangle |j\rangle |0\rangle. \quad (72)$$

Noting that $A_{i,j} = \langle s_j | i \rangle$, we compute the inner product of the n -qubit registers $|s_j\rangle$ and $|i\rangle$, which are computational basis states, and store the resulting binary outcome in the last qubit, thereby encoding $A_{i,j}$. More formally, the entry $A_{i,j}$ is computed as follows.

Lemma 22. *Let $|i\rangle$ and $|s_j\rangle$ be n -qubit computational basis states, and define $A_{i,j} = \langle s_j | i \rangle \in \{0, 1\}$. Then there exists a unitary $U_{i,j}$ acting on an $2n + 1$ -qubit register such that*

$$U_{i,j}(|i\rangle |s_j\rangle |0\rangle) = |i\rangle |s_j\rangle |A_{i,j}\rangle.$$

Moreover, $U_{i,j}$ can be implemented using $\mathcal{O}(n)$ CNOT gates, $\mathcal{O}(n)$ σ_X gates, $\mathcal{O}(n)$ Toffoli gates and possibly $\mathcal{O}(n)$ ancilla qubits.

Proof. For $r = 1, \dots, n$, apply a CNOT gate with the r -th qubit of $|i\rangle$ as the control and the r -th qubit of $|s_j\rangle$ as the target. After this operation, the r -th qubit of $|s_j\rangle$ stores $i_r \oplus s_{j,r}$. Next, apply a σ_X gate to each qubit of $|s_j\rangle$ to obtain i_r XNOR $s_{j,r}$. Each qubit of $|s_j\rangle$ then stores 1 if $i_r = s_{j,r}$ and 0 otherwise. Finally, apply a C^n -AND gate with the n qubits of $|s_j\rangle$ as controls and the last qubit as the target. This sets the last qubit to 1 if and only if all transformed qubits of $|s_j\rangle$ are equal to 1. Hence, the last qubit correctly encodes $A_{i,j}$. The procedure uses $\mathcal{O}(n)$ CNOT gates, $\mathcal{O}(n)$ σ_X gates, and a single C^n -AND gate, which can be implemented using $\mathcal{O}(n)$ Toffoli gates and, if necessary, $\mathcal{O}(n)$ ancilla qubits. \square

Consider the vector

$$\vec{c}_s = (c_0^{s_0}, c_1^{s_1}, \dots, c_{2^n-1}^{s_{2^n-1}}) \quad (73)$$

where $c_i^{s_i}$ denotes the number of occurrences of s_i in \vec{s} . Noting that $M_{\vec{s}}$ is a 1-column sparse matrix and a $\|\vec{c}_s\|_\infty$ -row sparse matrix, we can construct a $\mathcal{O}(\sqrt{\|\vec{c}_s\|_\infty}, n + 3, 0)$ block-encoding of $M_{\vec{s}}$ by invoking Lemma 5.

Remark 23. The computational cost of the oracle for $M_{\vec{s}}$ discussed above is evaluated under the assumption that $m = n$. In what follows, m is treated as a free parameter with $m \geq n$. Under this assumption, the computational complexity of implementing the block encoding described in Lemma 22 does not affect the overall computational complexity of the algorithm derived in Theorem 24. Accordingly, it is omitted from the subsequent complexity analysis.

4.4. Assembly via LCU. The final step is to implement $\sum_{r=0}^{K-1} D_{\vec{u}_r} F_{\vec{s}} D_{\vec{v}_r}$ via a quantum circuit. This is achieved by combining the block encodings constructed above with the LCU algorithm. In Theorem 24, we present this procedure and derive the corresponding non-asymptotic complexity of the algorithm.

Theorem 24. *Let $n, m, p, K \in \mathbb{N}$ with $m \geq n$. There exists a quantum circuit, V_{Π} , implementing a block encoding of $\sum_{r=0}^{K-1} D_{\vec{u}_r} F_{\vec{s}} D_{\vec{v}_r}$ with normalization factor*

$$\alpha := K \sqrt{\|\vec{c}_s\|_\infty} \sum_{r=0}^{K-1} \|\vec{\alpha}'_r\|_1. \quad (74)$$

and $\mathcal{O}(n + \log K)$ ancilla qubits. In other words, we have

$$(|0\rangle^{\mathcal{O}(n+\log K)} \otimes I_{2^n}) V_{\Pi} (|0\rangle^{\mathcal{O}(n+\log K)} \otimes I_{2^n}) = \frac{1}{\alpha} \sum_{r=0}^{K-1} D_{\vec{u}_r} F_{\vec{s}} D_{\vec{v}_r}. \quad (75)$$

The circuit uses $\mathcal{O}(m + n + p + \log K)$ qubits, $\mathcal{O}(n + \log K)$ Hadamard gates, $\mathcal{O}(m + p^2)$ CNOT gates, $\mathcal{O}(m)$ Toffoli gates, $\mathcal{O}(m)$ σ_X gates, and $\mathcal{O}(p + m + n^2)$ single-qubit controlled rotation gates. The circuit depth is $\mathcal{O}(m + p \log p + \log K)$.

Proof. Fix $r \in \{0, \dots, K-1\}$. Prepare two single-qubit ancilla registers a_r and b_r together with an n -qubit system register. Observe that $I_{a_r} \otimes I_{b_r} \otimes U_{\text{QFT}}$ is a $(1, 2, 0)$ block encoding of U_{QFT} . By repeated application of Lemma 4, the unitary

$$U_r := (I_{b_r} \otimes U_{\vec{u}_r})(I_{a_r} \otimes I_{b_r} \otimes U_{\text{QFT}})(I_{a_r} \otimes U_{\vec{v}_r}) \quad (76)$$

is a $(\|\vec{\alpha}'_r\|_1, 2, 0)$ block encoding of $D_{\vec{u}_r} F D_{\vec{v}_r}$. Using the construction described above for $M_{\vec{s}}$ and again invoking Lemma 4, we obtain a

$$(\|\vec{\alpha}'_r\|_1 \sqrt{\|\vec{c}_s\|_\infty}, n+5, 0) \quad (77)$$

block encoding of $D_{\vec{u}_r} F M_{\vec{s}} D_{\vec{v}_r}$, which we continue to denote by U_r . To implement the sum $\sum_{r=0}^{K-1} D_{\vec{u}_r} F M_{\vec{s}} D_{\vec{v}_r}$, we apply the LCU algorithm. Introduce $\mathcal{O}(\log K)$ ancilla qubits and define the select oracle

$$\text{SEL} = \sum_{r=0}^{K-1} U_r \otimes |r\rangle \langle r|. \quad (78)$$

To implement the linear combination of unitaries (LCU), we assume access to a separate state-preparation oracle $\text{PREP} := H^{\otimes \mathcal{O}(\log K)}$. Conjugating SEL with PREP yields the standard LCU unitary. The resulting construction is therefore a

$$\left(\sum_{r=0}^{K-1} K \sqrt{\|\vec{c}_s\|_\infty} \|\vec{\alpha}'_r\|_1, n+5+\log K, 0 \right) \quad (79)$$

block encoding of $\sum_{r=0}^{K-1} D_{\vec{u}_r} F M_{\vec{s}} D_{\vec{v}_r}$ [33, Lemma 52]. The stated gate counts, qubit complexity, and circuit depth follow from the previous complexity estimates, taking into account the costs of implementing each U_r as well as the overhead introduced by the LCU construction. \square

Note that the $\mathcal{O}(n^2)$ term in the expression $\mathcal{O}(p+n^2)$ in Theorem 24 arises from the requirement to apply $\mathcal{O}(n^2)$ controlled-rotation gates in the standard quantum circuit implementation of the Quantum Fourier Transform. We therefore observe that this quadratic dependence constitutes the dominant contribution to the overall gate-complexity estimates.

5. ERROR ANALYSIS

We now present an error analysis of the quantum algorithm implementing the Type-II NUFT.

5.1. Error Sources. We first identify the sources of error arising in the quantum implementation of the algorithm.

- (1) **Truncation Error.** Antolín and Townsend [14] approximate the NUFT matrix by a rank- K matrix from a Chebyshev expansion. To achieve $\|\cdot\|_{\max} \leq \epsilon_{\text{trunc}}$, choose $K = \mathcal{O}\left(\frac{\log(1/\epsilon'_{\text{trunc}})}{\log \log(1/\epsilon'_{\text{trunc}})}\right)$, for some $\epsilon'_{\text{trunc}} > 0$.
- (2) **Finite-Precision Oracle Error.** The sampling points t_j and s_j are given with m -bit precision, introducing errors in $t_j - s_j/N$ that propagate to the complex exponentials and Chebyshev evaluations.
- (3) **Arccosine Evaluation Error.** Implementing QSP requires rotations about the X axis with angles of the form $\arccos(x)$. Computing $\arccos(x)$ to p -bit precision introduces an approximation error of order $\mathcal{O}(2^{-p})$.
- (4) **Block-Encoding Error.** These errors accumulate in the block encoding of the constructed operators, reducing the overall accuracy of the resulting unitaries.

5.2. Error Bounds. We now bound the total error of the quantum algorithm and specify the parameters (K, m, p) so that the total error remains below the prescribed tolerance ϵ . Let \tilde{V}_{II} denote the approximately constructed version of the quantum circuit introduced in Theorem 24. Moreover, recall that we have approximated $F_{\text{II}} = A \circ (FM_{\bar{s}})$ on a quantum computer by implementing

$$\tilde{F}_{\text{II}} := A_K \circ (FM_{\bar{s}}) = \sum_{r=0}^{K-1} D_{\tilde{u}_r} F M_{\bar{s}} D_{\tilde{v}_r}. \quad (80)$$

To bound the total error, we apply the triangle inequality

$$\|\tilde{V}_{\text{II}} - F_{\text{II}}\| \leq \|\tilde{F}_{\text{II}} - F_{\text{II}}\| + \|\tilde{V}_{\text{II}} - \tilde{F}_{\text{II}}\| \quad (81)$$

The first term is determined by the truncation error. It has already been analyzed in [14] in the $\|\cdot\|_{\max}$ norm. We now derive an estimate for it in the $\|\cdot\|$ norm based on the following lemma.

Lemma 25. *Let $B, C \in \mathbb{C}^{N \times N}$. We have*

$$\|B \circ C\| \leq \sqrt{N} \|B\|_{\max} \|C\|. \quad (82)$$

Proof. Let e_1, \dots, e_N be the standard basis vectors in \mathbb{C}^N , and let $v = \sum_{i=1}^N v_i e_i$ be any vector. For each i , we have

$$\|(B \circ C)e_i\|_2 \leq \|B\|_{\max} \|Ce_i\|_2 \leq \|B\|_{\max} \|C\| \quad (83)$$

because $(B \circ C)e_i$ is obtained from Ce_i by multiplying each entry by a scalar of magnitude at most $\|B\|_{\max}$. By linearity and the triangle inequality, we have

$$\|(B \circ C)v\|_2 = \left\| \sum_{i=1}^N v_i (B \circ C)e_i \right\|_2 \leq \sum_{i=1}^N |v_i| \|(B \circ C)e_i\|_2 \leq \|B\|_{\max} \|C\| \|v\|_1. \quad (84)$$

Since $\|v\|_1 \leq \sqrt{N} \|v\|_2$, we obtain

$$\|(B \circ C)v\|_2 \leq \sqrt{N} \|B\|_{\max} \|C\| \|v\|_2 \quad (85)$$

for all $v \in \mathbb{C}^N$. The claim follows. \square

We can use Lemma 25 to compute an upper bound on K . This is carried out in Theorem 28 below. Next, we bound the second term in Equation (81), which will be used to determine the values of m and p in Theorem 28. We assume that the block-encoding of $M_{\bar{s}}$ is exact. This assumption is justified because we have black-box access to the oracle O_r , and the oracles O_c and O_A (Lemma 22) are constructed exactly. Furthermore, we assume that the quantum Fourier transform is implemented exactly, as we analyze the algorithm within the fault-tolerant regime. Define the normalization factors as $\alpha_{\tilde{u}_r} = \|\tilde{\alpha}'_r\|_1$ and $\alpha_{\tilde{v}_r} = 1$, where $\tilde{\alpha}'_r$ are the coefficients appearing in Equation (47). The analysis in the previous section implies that $U_{\tilde{u}_r}$ and $U_{\tilde{v}_r}$ are exact block-encodings.

$$U_{\tilde{u}_r} = \begin{pmatrix} D_{\tilde{u}_r}/\alpha_{\tilde{u}_r} & * \\ * & * \end{pmatrix}, \quad U_{\tilde{v}_r} = \begin{pmatrix} D_{\tilde{v}_r}/\alpha_{\tilde{v}_r} & * \\ * & * \end{pmatrix}. \quad (86)$$

Since the errors introduced above render the block-encodings inexact in the construction of \tilde{V}_{II} , let $\tilde{U}_{\tilde{u}_r}$ and $\tilde{U}_{\tilde{v}_r}$ be the implemented block-encodings such that

$$\tilde{U}_{\tilde{u}_r} = \begin{pmatrix} \tilde{D}_{\tilde{u}_r}/\alpha_{\tilde{u}_r} & * \\ * & * \end{pmatrix}, \quad \tilde{U}_{\tilde{v}_r} = \begin{pmatrix} \tilde{D}_{\tilde{v}_r}/\alpha_{\tilde{v}_r} & * \\ * & * \end{pmatrix}, \quad (87)$$

with $\tilde{D}_{\tilde{u}_r}$ and $\tilde{D}_{\tilde{v}_r}$ obtained via finite-precision oracle access and approximate function evaluation. Let \tilde{F} and $\tilde{M}_{\bar{s}}$ denote the corresponding exact block-encodings of F and $M_{\bar{s}}$, respectively. Note that \tilde{V}_{II} can be written as

$$\tilde{V}_{\text{II}} = \sum_{r=0}^{K-1} \tilde{D}_{\tilde{u}_r} \tilde{F} \tilde{M}_{\bar{s}} \tilde{D}_{\tilde{v}_r}. \quad (88)$$

The normalization factor $1/\alpha$, defined in Equation (74), is omitted in the following analysis, as it affects only the post-selection success probability. We bound the unitary circuit synthesis error of the unnormalized top-left block in order to determine the required parameters (K, m, p) as functions of the target precision. We have

$$\|\tilde{V}_{\text{II}} - \tilde{F}_{\text{II}}\| = \left\| \sum_{r=0}^{K-1} \tilde{D}_{\tilde{u}_r} \tilde{F} \tilde{M}_{\tilde{s}} \tilde{D}_{\tilde{v}_r} - \sum_{r=0}^{K-1} D_{\tilde{u}_r} F M_{\tilde{s}} D_{\tilde{v}_r} \right\|, \quad (89)$$

$$\leq \sum_{r=0}^{K-1} \|(\tilde{D}_{\tilde{u}_r} - D_{\tilde{u}_r}) \tilde{F} \tilde{M}_{\tilde{s}} \tilde{D}_{\tilde{v}_r}\| + \sum_{r=0}^{K-1} \|D_{\tilde{u}_r} F M_{\tilde{s}} (\tilde{D}_{\tilde{v}_r} - D_{\tilde{v}_r})\|. \quad (90)$$

Here, the terms involving $\tilde{F} - F$ and $\tilde{M}_{\tilde{s}} - M_{\tilde{s}}$ vanish because we assume that $\|\tilde{M}_{\tilde{s}} - M_{\tilde{s}}\| = 0 = \|\tilde{F} - F\|$. Note that $\|F\| = \|\tilde{F}\| = 1$, $\|M_{\tilde{s}}\| = \|\tilde{M}_{\tilde{s}}\| = \sqrt{\|\vec{c}_s\|_\infty}$, $\|D_{\tilde{u}_r}\| \leq \|\vec{\alpha}'_r\|_1$ and $\|D_{\tilde{v}_r}\| \leq 1$. Hence, we have

$$\|\tilde{V}_{\text{II}} - \tilde{F}_{\text{II}}\| \leq \sqrt{\|\vec{c}_s\|_\infty} \sum_{r=0}^{K-1} \left(\|\tilde{D}_{\tilde{u}_r} - D_{\tilde{u}_r}\| + \|\vec{\alpha}'_r\|_1 \|\tilde{D}_{\tilde{v}_r} - D_{\tilde{v}_r}\| \right). \quad (91)$$

Since we have

$$\|D_{\tilde{v}_r} - \tilde{D}_{\tilde{v}_r}\| = \max_j |(\tilde{v}_r)_j - (\tilde{v}_r)_j|, \quad \|D_{\tilde{u}_r} - \tilde{D}_{\tilde{u}_r}\| = \max_j |(\tilde{u}_r)_j - (\tilde{u}_r)_j|, \quad (92)$$

it suffices to bound the worst-case scalar error in a single diagonal entry. We first compute the error in the evaluation of the complex exponential and the Chebyshev polynomials, which will allow us to determine the worst-case scalar error in a single diagonal entry. We first bound the complex exponential term. In what follows, we assume that $m \geq n + 1$. In this case, the oracle constructing s_j is exact; hence, the only source of error is in t_j .

Lemma 26. *Let $m, n \in \mathbb{N}$ such that $m \geq n + 1$ and $N = 2^n$. Let $y_j = t_j - s_j/N$ for $j = 0, \dots, N - 1$, where t_j and s_j are provided by m -bit precision oracles. Let \tilde{y}_j denote the m -bit approximation of y_j . The errors in the complex exponential satisfy*

$$|e^{-i\pi N y_j} - e^{-i\pi N \tilde{y}_j}| \leq \pi N 2^{-m+1} \quad (93)$$

uniformly in j .

Proof. We have $|t_j - \tilde{t}_j| \leq 2^{-m}$. Hence, we have

$$|e^{-i\pi N y_j} - e^{-i\pi N \tilde{y}_j}| = \left| e^{-i\pi N (t_j - s_j/N)} - e^{-i\pi N (\tilde{t}_j - s_j/N)} \right| \quad (94)$$

$$\leq \pi N |(t_j - s_j/N) - (\tilde{t}_j - s_j/N)| \leq \pi N 2^{-m} \quad (95)$$

uniformly in j . \square

We now bound the error in the Chebyshev polynomials. Note that the Chebyshev polynomials are evaluated at two inputs, $x_j := 2j/N - 1$ and $y_j := (t_j - s_j/N)$. Since $j = 0, \dots, N - 1$, the values $2j/N - 1$ can be computed exactly (see Proposition 11), as we use at least n qubits. On the other hand, there is an approximation error in computing $t_j - s_j/N$ via the oracles. Hence, we treat these cases separately below. In Lemma 27, we continue to denote $y_j = 2N(t_j - \frac{s_j}{N})$ for simplicity.

Lemma 27. *Let $m, n \in \mathbb{N}$ such that $m \geq n + 1$. Let $q \leq K$ and $j = 0, \dots, N - 1$. Let $T_q(y_j) = \cos(q \arccos(y_j))$ denote the degree- q Chebyshev polynomial of the first kind. The errors in computing the Chebyshev polynomials can be bounded as follows:*

- (1) For $x_j = 2j/N - 1$, the error in the QSP implementation due to p -bit finite-precision evaluation of $\arccos(x)$ satisfies

$$|T_q(x_j) - \widehat{T}_q(x_j)| \leq q2^{-p+1} \leq K2^{-p+1}, \quad (96)$$

uniformly in j .

- (2) For $y_j = 2N(t_j - s_j/N)$, where t_j and s_j are provided by m -bit precision oracles, let \widehat{y}_j denote the m -bit approximation. Let $y_j^* \in (\min(y_j, \widehat{y}_j), \max(y_j, \widehat{y}_j))$. The total Chebyshev polynomial error satisfies

$$|T_q(y_j) - \widehat{T}_q(y_j)| \leq q \left(2^{-p+1} + \frac{N2^{-m+1}}{\sqrt{1 - (y_j^*)^2}} \right) \leq K \left(2^{-p+1} + \frac{N2^{-m+1}}{\sqrt{1 - (y_j^*)^2}} \right). \quad (97)$$

Proof. Let $\theta_j = \arccos(\cdot)$, where the argument is either x_j or y_j , and define $\delta_{\theta_j} := |\theta_j - \widehat{\theta}_j|$.

- (1) Let $x_j = 2j/N - 1$. The only source of error is the finite-precision evaluation of $\arccos(x_j)$ to p bits, giving a rotation-angle error $\delta_{\theta_j} \leq 2^{-p+1}$. By the mean-value theorem for the cosine function, the Chebyshev polynomial error is bounded by

$$|T_q(x_j) - \widehat{T}_q(x_j)| = |\cos(q\theta_j) - \cos(q(\theta_j + \delta_{\theta_j}))| \leq q\delta_{\theta_j} \leq q2^{-p+1} \leq K2^{-p+1}. \quad (98)$$

- (2) Let $y_j = 2N(t_j - s_j/N)$, where t_j and s_j/N are provided by an m -bit precision oracle. We have $|y_j - \widehat{y}_j| \leq 2N2^{-m} = N2^{-m+1}$. The rotation angle is $\theta_j = \arccos(y_j)$, while the computed rotation is $\widehat{\theta}_j$ with finite-precision p -bit evaluation. Applying the mean-value theorem to \arccos , there exists $y_j^* \in (\min(y_j, \widehat{y}_j), \max(y_j, \widehat{y}_j))$ such that

$$|\theta_j - \arccos(\widehat{y}_j)| \leq \frac{|y_j - \widehat{y}_j|}{\sqrt{1 - (y_j^*)^2}} \leq \frac{N2^{-m+1}}{\sqrt{1 - (y_j^*)^2}}. \quad (99)$$

Let $\widehat{\theta}_j = \arccos(\widehat{y}_j)$. By the triangle inequality, we have

$$\delta_{\theta_j} = |\theta_j - \widehat{\theta}_j| \leq |\theta_j - \arccos(\widehat{y}_j)| + |\arccos(\widehat{y}_j) - \widehat{\theta}_j| \leq \frac{N2^{-m+1}}{\sqrt{1 - (y_j^*)^2}} + 2^{-p+1}, \quad (100)$$

Applying the mean-value theorem to the cosine function,

$$|T_q(y_j) - \widehat{T}_q(y_j)| = |\cos(q\theta_j) - \cos(q\widehat{\theta}_j)| \leq q\delta_{\theta_j} = q \left(2^{-p+1} + \frac{N2^{-m+1}}{\sqrt{1 - (y_j^*)^2}} \right). \quad (101)$$

Since the maximum Chebyshev degree in the truncated expansion is $q \leq K$, the error is bounded by

$$|T_q(y_j) - \widehat{T}_q(y_j)| \leq K \left(2^{-p+1} + \frac{N2^{-m+1}}{\sqrt{1 - (y_j^*)^2}} \right). \quad (102)$$

This completes the proof. \square

We can now compute $\|D_{\vec{v}_r} - \widetilde{D}_{\vec{v}_r}\|$ and $\|D_{\vec{u}_r} - \widetilde{D}_{\vec{u}_r}\|$. Using Lemma 27, we have

$$\|D_{\vec{v}_r} - \widetilde{D}_{\vec{v}_r}\| \leq \begin{cases} 0, & r = 0, \\ r2^{-p+1}, & r \geq 1, \end{cases}. \quad (103)$$

Similarly, using Lemma 26, and Lemma 27, we have

$$\|D_{\vec{u}_r} - \widetilde{D}_{\vec{u}_r}\| \leq \|\vec{\alpha}'_r\|_1 \left(\pi N 2^{-m} + K \left(2^{-p+1} + \max_j \frac{N2^{-m+1}}{\sqrt{1 - (y_j^*)^2}} \right) \right), \quad (104)$$

Let $\alpha' = \sum_{r=0}^{K-1} \|\tilde{\alpha}'_r\|_1$. Substituting the bounds in Equation (91), we have

$$\|\tilde{V}_{\text{II}} - \tilde{F}_{\text{II}}\| \leq \sqrt{\|\vec{c}_s\|_\infty} \sum_{r=0}^{K-1} \|\tilde{\alpha}'_r\|_1 \left(\pi N 2^{-m} + K 2^{-p+1} + \max_j \frac{NK 2^{-m+1}}{\sqrt{1 - (y_j^*)^2}} + K 2^{-p+1} \right), \quad (105)$$

$$= \alpha' \sqrt{\|\vec{c}_s\|_\infty} \left(\pi N 2^{-m} + K 2^{-p+2} + \max_j \frac{NK 2^{-m+1}}{\sqrt{1 - (y_j^*)^2}} \right). \quad (106)$$

We can now complete our error analysis by specifying the parameters (K, m, p) so that the total error remains below the prescribed tolerance ϵ .

Theorem 28. *Let $\epsilon > 0$ and let $n, m, p, K \in \mathbb{N}$ with $m \geq n + 1$ and $N = 2^n$. Let $\tilde{V}_{\text{II}} = \sum_{r=0}^{K-1} \tilde{D}_{\tilde{u}_r} \tilde{F} \tilde{M}_{\tilde{s}} \tilde{D}_{\tilde{v}_r}$ denote the quantum implementation of the Type-II NUQFT with Chebyshev truncation degree K , m -bit oracle precision, and p -bit finite-precision evaluation of $\arccos(x)$ in the QSP implementation. Let $\|\tilde{\alpha}'_r\|_1 = \sum_{q=0}^{K-1} |\alpha'_{qr}|$, where α'_{qr} is defined in Equation (34). Define*

$$\alpha' = \sum_{r=0}^{K-1} \|\tilde{\alpha}'_r\|_1, \quad y_j = 2N(t_j - s_j/N), \quad y_j^* \in (\min(y_j, \hat{y}_j), \max(y_j, \hat{y}_j)), \quad (107)$$

where \hat{y}_j is a m -bit approximation of y_j . If (K, m, p) are chosen such that

$$K = \mathcal{O} \left(\frac{\log(\sqrt{N} \|\vec{c}_s\|_\infty / \epsilon)}{\log \log(\sqrt{N} \|\vec{c}_s\|_\infty / \epsilon)} \right), \quad (108)$$

$$m = \left\lceil \log_2 \frac{8\alpha' \sqrt{\|\vec{c}_s\|_\infty} (\pi N + K \max_j (1 - (y_j^*)^{-1/2}))}{\epsilon} \right\rceil, \quad (109)$$

$$p = \left\lceil \log_2 \frac{16\alpha' \sqrt{\|\vec{c}_s\|_\infty} K}{\epsilon} \right\rceil, \quad (110)$$

then the total error of the quantum algorithm satisfies

$$\|\tilde{V}_{\text{II}} - F_{\text{II}}\| \leq \epsilon. \quad (111)$$

In particular, it suffices to choose m and p such that

$$m = \mathcal{O} \left(\log \left(\frac{K \sqrt{\|\vec{c}_s\|_\infty} (N + K \max_j (1 - (y_j^*)^{-1/2}))}{\epsilon} \right) \right), \quad (112)$$

$$p = \mathcal{O} \left(\log \left(\frac{\sqrt{\|\vec{c}_s\|_\infty} K^2}{\epsilon} \right) \right). \quad (113)$$

Proof. We have

$$\|\tilde{V}_{\text{II}} - F_{\text{II}}\| \leq \underbrace{\|\tilde{F}_{\text{II}} - F_{\text{II}}\|}_{\text{truncation error}} + \underbrace{\|\tilde{V}_{\text{II}} - \tilde{F}_{\text{II}}\|}_{\text{block-encoding error}}, \quad (114)$$

where the first term is the Chebyshev truncation error and the second term is the block-encoding error. Using Lemma 25, the first term in Equation (81) can be expressed as

$$\|\tilde{F}_{\text{II}} - F_{\text{II}}\| = \|(A - A_K) \circ (FM_{\tilde{s}})\| \quad (115)$$

$$\leq \sqrt{N} \|A - A_K\|_{\max} \|FM_{\tilde{s}}\| \quad (116)$$

$$\leq \|\vec{c}_s\|_\infty \sqrt{N} \|A - A_K\|_{\max}. \quad (117)$$

The last equality follows since F is unitary, and we have

$$\|FM_{\tilde{s}}\| = \|M_{\tilde{s}}\| = \sqrt{\|\vec{c}_s\|_\infty}. \quad (118)$$

Hence, in order to ensure that $\|\tilde{F}_{\text{II}} - F_{\text{II}}\| \leq \epsilon/2$ for some $\epsilon > 0$, it suffices to choose $\epsilon'_{\text{trun}} = \epsilon/2\sqrt{N\|\vec{c}_s\|_\infty}$. Hence, it suffices to choose K such that

$$K = \mathcal{O}\left(\frac{\log(\sqrt{N\|\vec{c}_s\|_\infty}/\epsilon)}{\log\log(\sqrt{N\|\vec{c}_s\|_\infty}/\epsilon)}\right), \quad (119)$$

From (105), the block-encoding error satisfies

$$\|\tilde{V}_{\text{II}} - \tilde{F}_{\text{II}}\| \leq \alpha'\sqrt{\|\vec{c}_s\|_\infty} \left(\pi N 2^{-m} + K 2^{-p+2} + \max_j \frac{NK 2^{-m+1}}{\sqrt{1-(y_j^*)^2}} \right). \quad (120)$$

Let $C := \alpha'\sqrt{\|\vec{c}_s\|_\infty}$ and $\kappa := \max_j \frac{1}{\sqrt{1-(y_j^*)^2}}$. Using this notation, Equation (120) can be succinctly expressed as

$$\|\tilde{V}_{\text{II}} - \tilde{F}_{\text{II}}\| \leq C(2^{-m}(\pi N + 2NK\kappa) + K 2^{-p+2}). \quad (121)$$

To ensure that the right-hand side is at most $\epsilon/2$, we can allocate the error budget equally between the oracle and QSP contributions, i.e.,

$$C 2^{-m}(\pi N + 2NK\kappa) \leq \frac{\epsilon}{4}, \quad (122)$$

$$CK 2^{-p+2} \leq \frac{\epsilon}{4}. \quad (123)$$

Solving for m , we obtain

$$C 2^{-m}(\pi N + 2NK\kappa) \leq \frac{\epsilon}{4} \iff m \geq \log_2 \left(\frac{4C(\pi N + 2NK\kappa)}{\epsilon} \right). \quad (124)$$

Solving for p , we obtain

$$CK 2^{-p+2} \leq \frac{\epsilon}{4} \iff 2^{-p} \leq \frac{\epsilon}{16CK} \iff p \geq \log_2 \left(\frac{16CK}{\epsilon} \right). \quad (125)$$

Substituting the definitions of C and κ yields

$$m = \left\lceil \log_2 \left(\frac{4\alpha'\sqrt{\|\vec{c}_s\|_\infty}(\pi N + 2NK \max_j (1 - (y_j^*)^{-1/2}))}{\epsilon} \right) \right\rceil, \quad (126)$$

$$p = \left\lceil \log_2 \left(\frac{16\alpha'\sqrt{\|\vec{c}_s\|_\infty}K}{\epsilon} \right) \right\rceil. \quad (127)$$

With these choices of m and p , the error satisfies $\|\tilde{V}_{\text{II}} - \tilde{F}_{\text{II}}\| \leq \epsilon$. Combined with the choice of K , we therefore have

$$\|\tilde{V}_{\text{II}} - F_{\text{II}}\| \leq \epsilon. \quad (128)$$

We now further simplify the choices of m and p . It is well known [56, 57] that for $\nu \geq 0$ and $0 \leq x \ll \nu$, we have

$$J_\nu(x) \sim \frac{(x/2)^\nu}{\Gamma(\nu+1)}, \quad (129)$$

where Γ is the Gamma function. Furthermore, recall that $\alpha'_{qr} = \mathcal{O}(\alpha_{qr})$ (see Equation (34)), where α_{qr} is defined in Equation (33) with $\gamma = \frac{1}{2}$ by

$$\alpha_{qr} = \begin{cases} 4i^r J_{\frac{q+r}{2}}(-\pi/4) J_{\frac{r-q}{2}}(-\pi/4), & \text{if } \text{mod}(|q-r|, 2) = 0, \\ 0, & \text{otherwise} \end{cases} \quad (130)$$

The condition $\text{mod}(|q-r|, 2) = 0$ implies that q and r have the same parity. Hence, the order of the Bessel function J is an integer in Equation (130). Since we are interested in $|\alpha_{qr}|$, it suffices to evaluate the Bessel functions at $\pi/4$ and to assume $(r-q)/2 \geq 0$, as Bessel functions of integer order are either even or odd. Equation (129) now implies that $|\alpha_{qr}| = \mathcal{O}(1)$, since for the fixed

value $x_0 = \pi/4$, the magnitude of $J_\nu(x_0)$ decreases rapidly as ν increases. Hence, $\alpha' = \mathcal{O}(K)$, since each of the K summands $|\alpha'_{qr}|$ is $\mathcal{O}(1)$. Based on Equation (126) and Equation (127), it suffices to choose m and p such that

$$m = \mathcal{O} \left(\log \left(\frac{NK \sqrt{\|\vec{c}_s\|_\infty} (1 + K \max_j (1 - (y_j^*)^{-1/2}))}{\epsilon} \right) \right), \quad p = \mathcal{O} \left(\log \left(\frac{\sqrt{\|\vec{c}_s\|_\infty} K^2}{\epsilon} \right) \right). \quad (131)$$

This completes the proof. \square

The expressions in Theorem 28 are rather involved. Noting that $N = 2^n$ and $\|\vec{c}_s\|_\infty = \mathcal{O}(2^n)$, we can further simplify the $\mathcal{O}(\cdot)$ estimates in Theorem 28 in terms of n , ϵ , and $\kappa := \max_j \frac{1}{\sqrt{1 - (y_j^*)^2}}$.

Noting that $\sqrt{N\|\vec{c}_s\|_\infty} = \mathcal{O}(2^n)$, we have

$$\log \left(\frac{\sqrt{N\|\vec{c}_s\|_\infty}}{\epsilon} \right) = \Theta(n) + \log \left(\frac{1}{\epsilon} \right) = \Theta \left(n + \log \left(\frac{1}{\epsilon} \right) \right). \quad (132)$$

Hence, we can simplify the complexity estimate for K in Equation (108) to

$$K = \mathcal{O} \left(\frac{n + \log(1/\epsilon)}{\log(n + \log(1/\epsilon))} \right) = \mathcal{O} \left(n + \log \left(\frac{1}{\epsilon} \right) \right). \quad (133)$$

Similarly, we obtain

$$p = \mathcal{O} (n + \log(1/\epsilon) + \log K), \quad (134)$$

$$= \mathcal{O} \left(n + \log \left(\frac{1}{\epsilon} \right) + \log \left(n + \log \left(\frac{1}{\epsilon} \right) \right) \right) = \mathcal{O} \left(n + \log \left(\frac{1}{\epsilon} \right) \right). \quad (135)$$

The second last equality follows since $\log K = \mathcal{O}(n + \log(1/\epsilon))$. In a similar manner, we obtain

$$m = \mathcal{O} \left(\log \left(\frac{NK \sqrt{\|\vec{c}_s\|_\infty} (1 + K\kappa)}{\epsilon} \right) \right), \quad (136)$$

$$= \mathcal{O} \left(\log \left(\frac{K 2^{3n/2} (1 + K\kappa)}{\epsilon} \right) \right), \quad (137)$$

$$= \mathcal{O} \left(\log K + n + \log(1 + K\kappa) + \log \left(\frac{1}{\epsilon} \right) \right) = \mathcal{O} \left(n + \log \left(\frac{1}{\epsilon} \right) + \log(1 + K\kappa) \right). \quad (138)$$

Corollary 29. *Let $\epsilon > 0$ and let $n, m, p, K \in \mathbb{N}$ with $m \geq n + 1$. Let \tilde{V}_{II} , y_j and y_j^* be defined as in Theorem 28. If the parameters (K, m, p) are chosen such that*

$$K, p = \mathcal{O} \left(n + \log \left(\frac{1}{\epsilon} \right) \right), \quad m = \mathcal{O} \left(n + \log \left(\frac{1}{\epsilon} \right) + \log(1 + K\kappa) \right), \quad (139)$$

where $\kappa := \max_j \frac{1}{\sqrt{1 - (y_j^*)^2}}$, then $\|\tilde{V}_{\text{II}} - F_{\text{II}}\| \leq \epsilon$.

Proof. This follows from Theorem 28 and the discussion above. \square

6. NUMERICAL RESULTS

We present numerical results obtained from both classical simulations and hybrid classical–quantum implementations for small-scale instances. The objective is to validate the new components introduced in the quantum algorithm rather than to re-establish the accuracy of the underlying classical method. The experiments therefore isolate the elements specific to our construction: the low-rank truncation used in the LCU representation, finite-precision discretization of node data, the reversible implementation of the arccos subroutine, the state-preparation routines $U_{v_{\vec{r}}}$ and $U_{u_{\vec{r}}}$, the small- K LCU combination, and the block encoding of the matrix $M_{\vec{g}}$. Accordingly, we run numerical tests for problem sizes accessible to classical simulation. The code used to generate the reported results is available in [58].

6.1. Validation of Low-Rank Truncation Error Scaling. The low-rank Chebyshev approximation underlying our construction was extensively analyzed and numerically validated in Antolín and Townsend [14]. As our work focuses on translating this decomposition into a quantum block-encoding framework, we do not repeat those experiments and instead only validate the truncation behavior of the low-rank approximation for representative node configurations. The low-rank truncation error is characterized by

$$\|\tilde{F}_{\text{II}}^{(K)} - F_{\text{II}}\| \leq \|\tilde{c}_s\|_{\infty} \sqrt{N} \|A - A_K\|_{\max}. \quad (140)$$

Here, the superscript indicates that $\tilde{F}_{\text{II}}^{(K)}$ is defined with respect to the truncation parameter K . While $\|A - A_K\|_{\max} = \mathcal{O}(\log(1/\epsilon))$, a more precise estimate is $5\gamma e^{W(\frac{\log(140/\epsilon)}{5\gamma})}$, as given in [25], where W is Lambert's W function. Hence, we obtain the estimate

$$K = 5\gamma e^{\left(\frac{\log(\|\tilde{c}_s\|_{\infty} \sqrt{N} 140/\epsilon)}{5\gamma}\right)}. \quad (141)$$

For a range of transform sizes N , we numerically construct $\tilde{F}_{\text{II}}^{(K)}$ for increasing K and measure the spectral-norm error $\|F_{\text{II}} - \tilde{F}_{\text{II}}^{(K)}\|$. The experiments cover perturbed equispaced grids, clustered nodes, and randomly distributed nodes in $[0, 1)$. Figure 6 confirms the predicted error baselines and shows that moderate K suffices to achieve $\epsilon = 10^{-10}$. This test also demonstrates that, for quantum implementations, the LCU qubit cost is modest. For instance, when $\epsilon = 10^{-5}$, approximately 4 qubits are required.

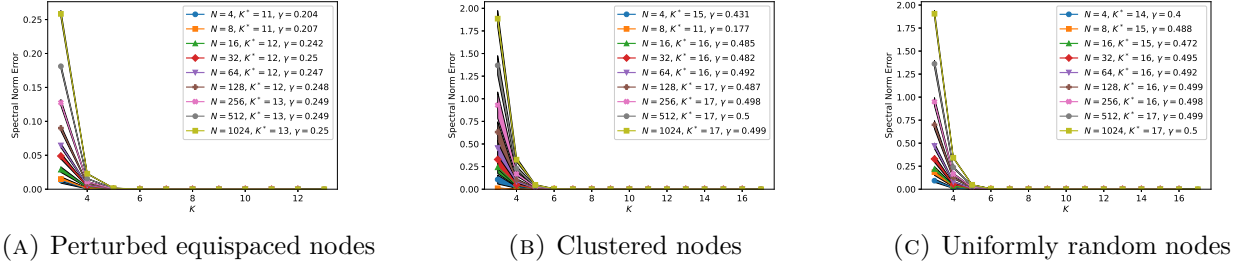


FIGURE 6. $\|(F_{\text{II}} - \tilde{F}_{\text{II}}^{(K)})\|_2$ as a function of K for $N = 2^n$, $n = 2, \dots, 10$, with accuracy $\epsilon = 10^{-10}$. For each N and node geometry, the error is averaged over 20 independent complex Gaussian test vectors. K^* denotes the minimal K required to achieve the prescribed tolerance.

The low-rank Chebyshev approximation underlying our construction was extensively analyzed and numerically validated in Antolín and Townsend [14]. As our work focuses on translating this decomposition into a quantum block-encoding framework, we do not repeat those experiments and instead validate the newly introduced quantum components.

6.2. Finite-Precision Effects. We next investigate the effect of finite-precision node representation on the accuracy of the transform. The parameter m governs the precision with which the non-uniform nodes t_j and derived quantities such as s_j are represented. In the theoretical analysis presented in Proposition 15, the parameter m scales logarithmically with the truncation parameter K and the condition parameter κ . The purpose of this experiment is to demonstrate that the dependence of m on both κ and K is sufficiently mild for practical purposes. This is verified through classical emulation. For a fixed transform size N , we generate node sets using a function parameterized by γ such that

$$\left|t_j - \frac{s_j}{N}\right| = \gamma N, \quad \gamma \in \left(0, \frac{1}{2}\right), \quad (142)$$

thereby producing a range of geometric configurations with varying κ . Given a node set $\{x_j\} \subseteq [0, 1)$, we can form the truncated representations

$$t_j^{(m)} = \frac{\text{round}(2^m t_j)}{2^m}, \quad (143)$$

and construct the corresponding approximate transform $\tilde{F}_{\Pi}^{(m)}$ using these discretized nodes. For each node set, we compute the parameter κ and the minimal precision m^* required to achieve spectral-norm error ϵ . The minimal precision m^* is determined via a bracketing and binary search procedure over m . As shown in Table 1, κ increases monotonically with γ , with particularly sharp growth once $\gamma \geq 0.49$. Despite this amplification, the required precision parameter m^* remains essentially stable across the entire range. This stability arises from compensating effects. Although κ grows rapidly near the boundary, its overall scaling remains moderate (effectively sublinear), and the admissible K also stays moderate. Most importantly, the precision depends on $\log(1 + K\kappa)$, whose logarithmic structure mitigates the impact of large κ . Consequently, even when κ becomes large, $\log(1 + K\kappa)$ grows slowly and m^* changes very little. Thus, the $\log(1 + K\kappa)$ factor in Proposition 15 is mild, and the parameters m, n, p all scale as $\mathcal{O}(n + \log(1/\epsilon))$ morally.

#	γ	κ	K	$\log(1 + K\kappa)$	m^*
1	0	1	1	0.693147	7
2	0.0544444	1.00598	10	2.40332	15
3	0.108889	1.02459	11	2.5072	15
4	0.163333	1.05804	13	2.69155	15
5	0.217778	1.11091	14	2.80655	15
6	0.272222	1.19218	14	2.87303	15
7	0.326667	1.32088	15	3.03559	15
8	0.381111	1.54484	16	3.24717	15
9	0.435556	2.0363	17	3.57283	15
10	0.49	5.02519	17	4.45931	15

TABLE 1. Comparison of κ and $\log(1 + K\kappa)$ for two γ regimes for $N = 2^6$, $\epsilon = 10^{-12}$.

6.3. Quantum Arccos Subroutine. We examine the quantum implementation of the arccos subroutine using a reversible CORDIC-style routine with precision parameter p . The $\arcsin(x)$ algorithm of [51] uses $5p - 1$ qubits, while our $\arccos(x)$ implementation requires $7p + 10$, preserving $\mathcal{O}(p)$ scaling but with a larger constant factor. Numerical tests with a **matrix-product-state simulator** for $p = 1, \dots, 6$ (with $m = 6$) show that $p = 7$ exceeds simulator capacity. Results for $p = 1, 3, 5$ are shown in Figure 7. These results indicate a hardware bottleneck that restricts the

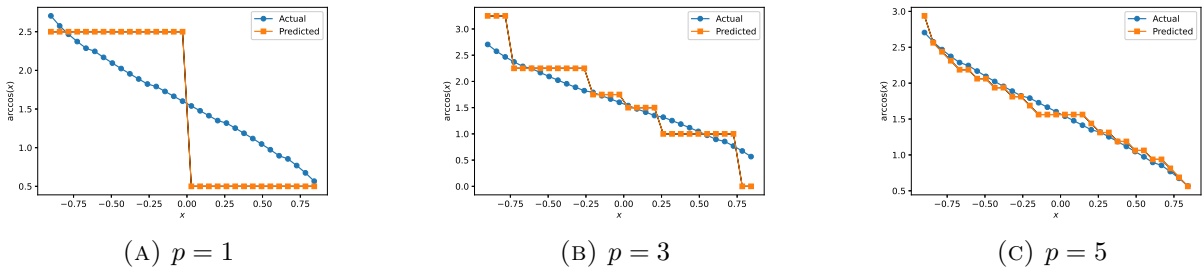


FIGURE 7. Comparison of actual and predicted values of $\arccos(x)$ for odd p values ($p = 1, 3, 5$). The corresponding mean absolute errors are 0.5195115053, 0.2251069658, and 0.0645826060, respectively.

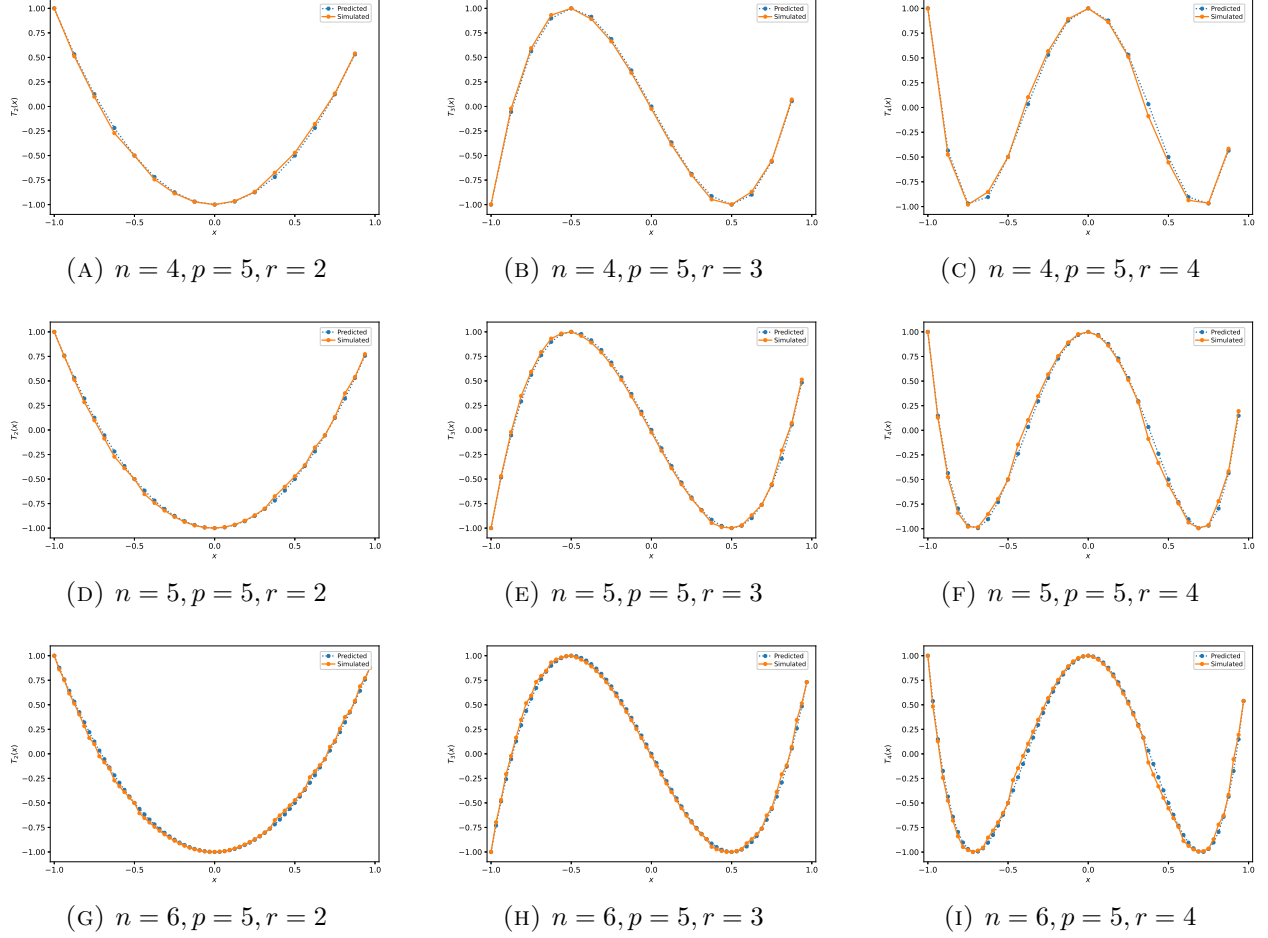


FIGURE 8. Comparison of computed and predicted outputs for different parameter of the quantum circuit $U_{v_{\vec{r}}}$ for $n \in \{4, 5, 6\}$ and $r \in \{2, 3, 4\}$ with fixed $p = 5$.

algorithm’s simulation to small parameters. Consequently, a fully quantum implementation is not feasible with current hardware. Therefore, we adopt a hybrid classical–quantum approach, performing arithmetic operations classically while enabling quantum simulation for small parameters.

6.4. Hybrid Implementation of $U_{v_{\vec{r}}}$. We validate the algorithm in Section 4.1 implementing the unitary operator $U_{v_{\vec{r}}}$. The arccos computation is performed classically due to current hardware and simulation constraints and is included in the pre-processing stage. The resulting parameters are then loaded into a p -qubit register. To verify correctness, the circuit is simulated for small problem sizes where full statevector simulation is feasible. The simulated amplitudes are renormalized by multiplying by \sqrt{N} and compared with the classical values $T_r(x_j)$ defining $v_{\vec{r}}$, computed via direct Chebyshev evaluation using NumPy. For various degrees r and qubit counts n , the simulated amplitudes are compared with the corresponding Chebyshev polynomial values. The results in Figure 8 show that $U_{v_{\vec{r}}}$ accurately reproduces the vector $v_{\vec{r}}$. Table 2 reports the statevector error for fixed $n = 4$ and $r = 4$ as p increases. The ratios of consecutive errors confirm that the error decreases by approximately a factor of two when p increases by one.

6.5. Hybrid Implementation of $U_{u_{\vec{r}}}$. We next validate the algorithm in Section 4.2 implementing the unitary operator $U_{u_{\vec{r}}}$. As in the previous analysis, all arithmetic computations are carried out classically, and the resulting data are subsequently loaded into the quantum registers. Let

#	n	p	r	Error	Ratio
1	4	1	4	0.9880609500	1.6475
2	4	2	4	0.5997170775	2.2256
3	4	3	4	0.2694581809	2.1944
4	4	4	4	0.1227710437	2.0449
5	4	5	4	0.0600312609	1.8409
6	4	6	4	0.0326167771	2.2405
7	4	7	4	0.0145581686	1.9220
8	4	8	4	0.0075722616	–

TABLE 2. Statevector error for fixed $n = 4$ and $r = 4$ as p increases.

$\vec{x} = \vec{t} - \vec{s}/N$ and

$$u_q(\vec{x}) = \sqrt{N} e^{-i\pi N \vec{x}} T_q(2N \vec{x}) \quad (144)$$

denote the normalized amplitude of the $|0\rangle$ computational basis state of the circuit U_q . For a range of values of q and transform sizes N , we plot the real and imaginary parts of the simulated amplitudes and the predicted components in Figure 9. The results in Figure 9 provide numerical evidence that U_q accurately reproduces $u_{qr}(\vec{x})/\sqrt{N}$. Table 3 reports the statevector error for fixed $n = 4$ and $q = 2$ as p, m increases.

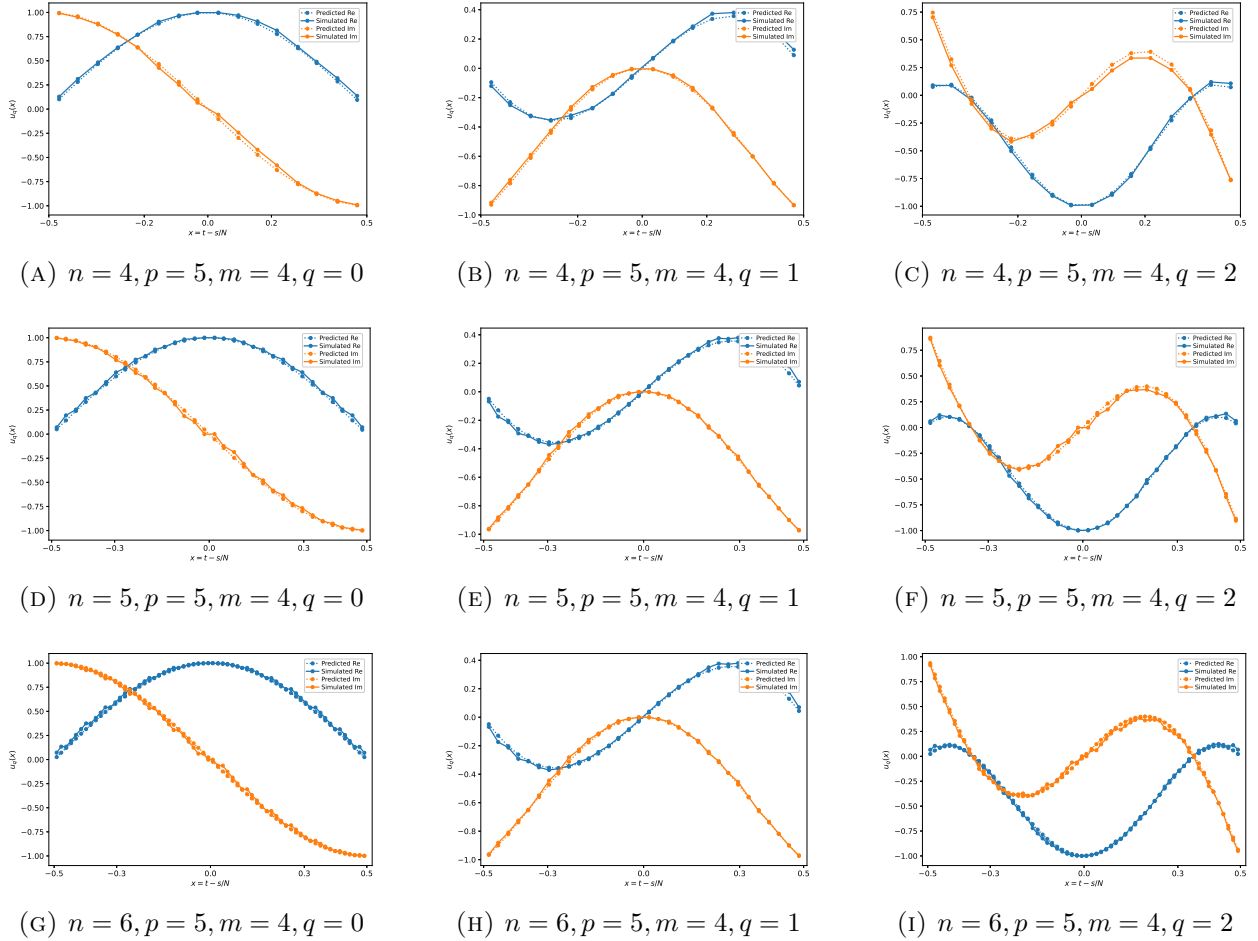


FIGURE 9. Comparison of computed and predicted outputs for different parameters of the quantum circuit U_q for $n \in \{4, 5, 6\}$ and $q \in \{0, 1, 2\}$ with $m = 4$ and $p = 5$.

#	n	m	p	q	Error	Ratio
1	4	2	1	2	1.6138906535	2.00799
2	4	2	2	2	0.8036549819	1.30723
3	4	2	3	2	0.6147763375	1.28833
4	4	2	4	2	0.4771891201	1.06065
5	4	2	5	2	0.4499019429	1.03347
6	4	2	6	2	0.4353344292	1.00562
7	4	2	7	2	0.4329028110	–

#	n	m	p	q	Error	Ratio
1	4	1	2	2	1.1343486555	1.41149
2	4	2	2	2	0.8036549819	1.12381
3	4	3	2	2	0.7151168695	1.04547
4	4	4	2	2	0.6840150547	1.01223
5	4	5	2	2	0.6757494378	1.00142
6	4	6	2	2	0.6747895628	1.00031
7	4	7	2	2	0.6745814549	–

TABLE 3. State-vector error for fixed $n = 4$ and $q = 2$. The left table varies p with $m = 2$ fixed, while the right table varies m with $p = 2$ fixed. The last column shows the ratio of consecutive rows.

We next validate $U_{u_{\vec{r}}} = \sum_{q=0}^{K-1} \alpha'_{qr} U_q$ using the LCU algorithm. Let

$$u_r(\vec{x}) = \sqrt{N} \|\vec{\alpha}_{qr}\|_1 \sum_{q=0}^{K-1} \alpha'_{qr} e^{-i\pi N \vec{x}} T_q(2N\vec{x}) \quad (145)$$

denote the normalized amplitude of the $|0\rangle$ basis state of the circuit $U_{u_{\vec{r}}}$. For $K = 2$, we report the results in Figure 10, which provide evidence that $U_{u_{\vec{r}}}$ accurately reproduces $u_r(\vec{x})/\|\alpha_{qr}\|_1\sqrt{N}$. Note that the LCU algorithm dominates the computational cost of implementing the method. This is because the LCU procedure requires multi-qubit controlled unitaries which, when decomposed into elementary gates, reduce to multi-qubit controlled- X gates, since the arithmetic loader ultimately consists of such operations. Given current simulation capabilities, this approach can only be implemented efficiently for small values of K and n . In particular, we restrict to the case $K = 2$.

6.6. Numerical Validation of the M_s Block Encoding. Lastly, we validate the block encoding constructed for the matrix $M_{\vec{s}}$. The implemented circuit exploits the structure of $M_{\vec{s}}$. Since each column has exactly one nonzero entry, the block encoding is realized via a simplified right-isometry. Although inspired by the sparse-access block-encoding lemma, the implementation does not explicitly realize the oracle triplet (O_c, O_r, O_A) . Instead, it uses the column structure of $M_{\vec{s}}$ to build a direct circuit. The resulting unitary $U_{M_{\vec{s}}}$ uses $n + 1$ ancilla qubits and satisfies

$$(|0\rangle^{n+1} \otimes I) U_{M_{\vec{s}}} (|0\rangle^{n+1} \otimes I) = \frac{M_{\vec{s}}}{\sqrt{d_r}}, \quad d_r = \|\vec{c}_s\|_{\infty}. \quad (146)$$

We verify Equation (146) by simulating $U_{M_{\vec{s}}}$, extracting the encoded matrix by projecting the ancilla register onto $|0\rangle^{n+1}$, and comparing it with the normalized target matrix $M_{\vec{s}}/\sqrt{d_r}$. We quantify the error using the maximum entrywise norm and the spectral norm. The construction is tested on representative vectors \vec{s} with different sparsity patterns:

- (1) **Identity:** $s_j = j$, yielding the identity matrix ($d_r = 1$).
- (2) **Bit-Reversal:** s_j is the bit-reversal of j (permutation, $d_r = 1$).
- (3) **Constant:** all entries of s are identical, giving maximal multiplicity $d_r = N$.
- (4) **Two-Cluster:** half the columns map to one row and half to another ($d_r = N/2$).
- (5) **Heavy Row:** most columns map to one row, with the remainder distributed.
- (6) **Random:** s_j sampled uniformly from $\{0, \dots, N - 1\}$.

We report representative results for system size $n = 5$ in Table 4. The extracted encoded block agrees with the expected matrix $M_s/\sqrt{d_r}$ to machine precision for all tested configurations.

Remark 30. The block encoding QFT is straightforward. A complete block encoding of the NUQFT matrix can be obtained by composing the components simulated above. We defer the full construction to future work, as the simulation becomes computationally expensive for large K .

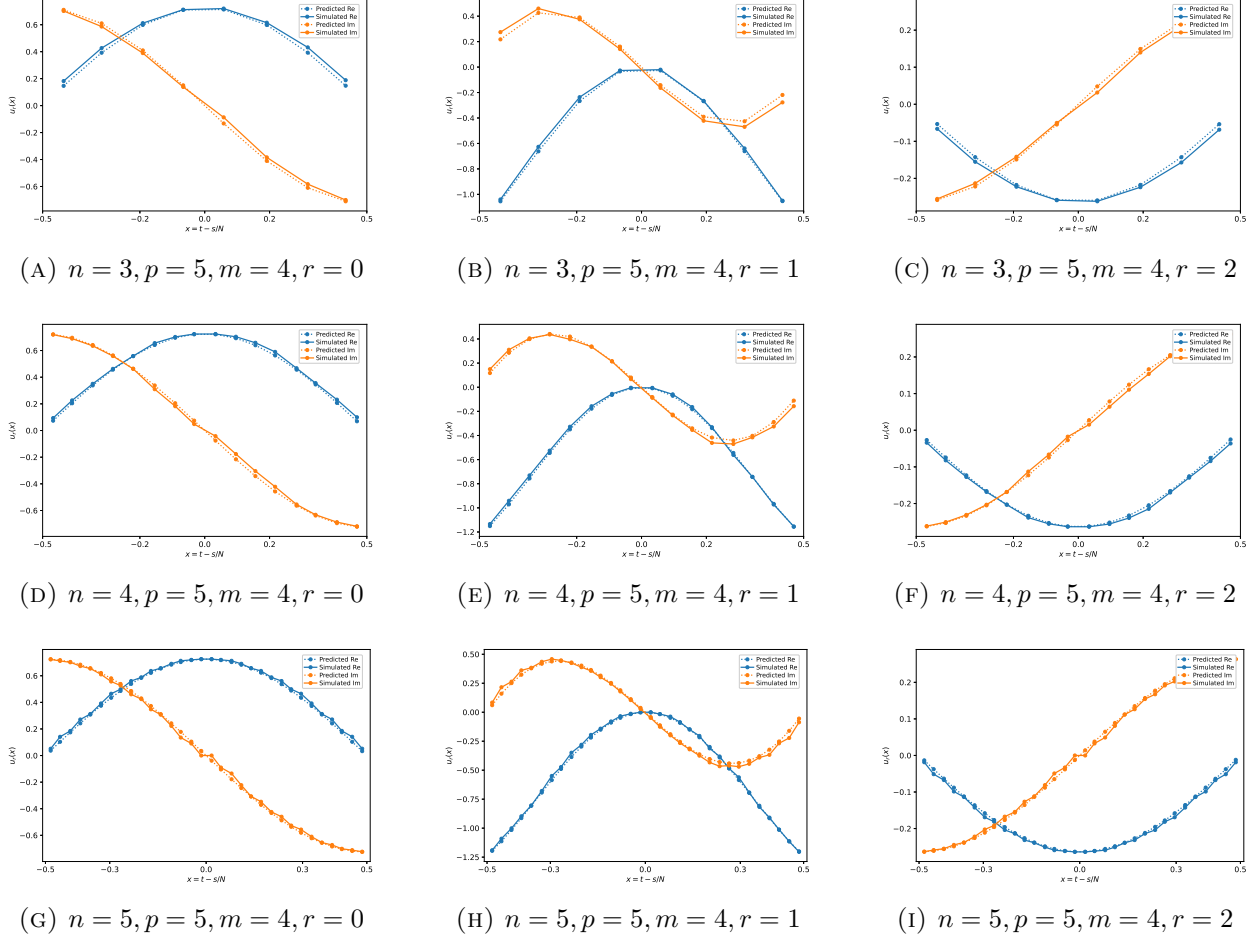


FIGURE 10. Comparison of the computed and predicted for different parameters of the quantum circuit U_{u_r} for $n \in \{4, 5, 6\}$ and $r \in \{0, 1, 2\}$ with $m = 4$ and $p = 5$.

#	Family	d_r	$\alpha = \sqrt{d_r}$	Max error	Spectral error
1	Identity	1	1.000000	0.0	0.0
2	Bit reversal	1	1.000000	0.0	0.0
3	Constant ($s_j = 0$)	32	5.656854	3.9×10^{-16}	1.7×10^{-15}
4	Constant ($s_j = N - 1$)	32	5.656854	3.9×10^{-16}	1.7×10^{-15}
5	Two cluster	16	4.000000	7.3×10^{-16}	2.0×10^{-15}
6	Heavy row	17	4.123106	6.9×10^{-16}	1.9×10^{-15}
7	Random	3	1.732051	1.6×10^{-14}	2.4×10^{-14}

TABLE 4. Numerical validation of the M_g block encoding for $n = 5$.

7. CONCLUSION

We have developed a quantum algorithm for implementing the Type-II non-uniform discrete Fourier transform (NUDFT), which can be readily extended to the Type-I and Type-III variants. We have also presented a rigorous error analysis that identifies the dominant sources of approximation error and derives explicit upper bounds on their respective contributions. The analysis shows that the required computational resources scale logarithmically with the inverse of the target precision and polynomially with the number of qubits.

7.1. **Future Directions.** We discuss below several future research directions:

- (1) The proposed NUQFT algorithm assumes oracle access to the non-uniform sampling points (cf. Assumption 12) and to the corresponding inverse mapping (cf. Assumption 21). An important direction for future work is to identify concrete computational scenarios in which such oracles can be implemented efficiently, either through explicit circuit constructions or through data-generation models where the required access arises naturally.
- (2) The present framework relies on Chebyshev polynomial approximations implemented via quantum signal processing. Alternative approximation strategies, including rational approximations, Fourier–Bessel expansions, or minimax constructions tailored to restricted domains, may offer improved constants or reduced ancilla usage. Exploring how such schemes can be incorporated into QSP or the more general QSVT framework may lead to more resource-efficient NUQFT implementations.
- (3) The analysis is carried out in a fault-tolerant setting with idealized primitives, including exact QFT implementations and perfect oracle access. Future work should address explicit compilation into standard fault-tolerant gate sets, with attention to optimizing T -count and T -depth, as well as adapting the construction to hardware constraints such as limited connectivity. Extending the framework to NISQ devices is another important direction. This includes incorporating approximate implementations of the Quantum Fourier Transform (QFT) and approximate rotations (see. Equation (54)) by eliminating small-angle rotations to reduce circuit depth.
- (4) The numerical experiments presented here are limited by the qubit counts and memory capacity of current quantum simulators and hardware. Future work may explore more scalable implementations. In particular, more resource-efficient realizations of key arithmetic primitives—especially the arccos subroutine and the LCU stage—could substantially reduce qubit and gate overhead. Possible directions include improved polynomial approximations, QSVT-based constructions, circuit-level optimizations, or hybrid LCU implementations. Such improvements could enable larger-scale realizations and provide a clearer evaluation of the practical performance of the proposed approach.
- (5) Many applications of non-uniform Fourier analysis arise in higher dimensions. Extending the NUQFT framework to multidimensional NUDFTs, for example via tensorized or separable low-rank decompositions, is therefore a natural next step. More broadly, the techniques developed here may generalize to other non-uniform integral transforms, including cosine and Laplace transforms, discrete Legendre transforms, and Fourier transforms defined on manifolds.
- (6) Finally, the NUQFT is intended to function as a subroutine within larger quantum algorithms rather than as an isolated primitive. Studying its integration into complete quantum workflows—including state preparation, intermediate processing, and measurement—remains an important open problem, particularly in identifying application domains where such integration yields a provable advantage.

REFERENCES

- [1] James W. Cooley and John W. Tukey. “An algorithm for the machine calculation of complex Fourier series”. In: *Mathematics of Computation* 19.90 (1965), pp. 297–301.
- [2] Li Tan and Jean Jiang. *Digital signal processing: fundamentals and applications*. Academic press, 2018.
- [3] Jie Shen, Tao Tang, and Li-Lian Wang. *Spectral methods: algorithms, analysis and applications*. Vol. 41. Springer Science & Business Media, 2011.
- [4] William L. Briggs and Van E. Henson. *The DFT: an owner’s manual for the discrete Fourier transform*. SIAM, 1995.
- [5] Sonali Bagchi and Sanjit K. Mitra. *The non-uniform discrete Fourier transform and its applications in signal processing*. Vol. 463. Springer Science & Business Media, 2012.

- [6] Chuan Qin, Chin-Chen Chang, and Pei-Ling Tsou. “Robust image hashing using non-uniform sampling in discrete Fourier domain”. In: *Digital Signal Processing* 23.2 (2013), pp. 578–585.
- [7] Qing Huo Liu, Xue Min Xu, Bo Tian, and Zhong Qing Zhang. “Applications of non-uniform fast transform algorithms in numerical solutions of differential and integral equations”. In: *IEEE Transactions on geoscience and remote sensing* 38.4 (2000), pp. 1551–1560.
- [8] Alok Dutt and Vladimir Rokhlin. “Fast Fourier transforms for non-equispaced data”. In: *SIAM Journal on Scientific computing* 14.6 (1993), pp. 1368–1393.
- [9] Antony F. Ware. “Fast approximate Fourier transforms for irregularly spaced data”. In: *SIAM Review* 40.4 (1998), pp. 838–856.
- [10] Daniel Potts, Gabriele Steidl, and Manfred Tasche. “Fast Fourier transforms for nonequispaced data: A tutorial”. In: *Modern Sampling Theory: Mathematics and Applications* (2001), pp. 247–270.
- [11] Jeffrey A. Fessler and Bradley P. Sutton. “Non-uniform fast Fourier transforms using min-max interpolation”. In: *IEEE transactions on signal processing* 51.2 (2003), pp. 560–574.
- [12] Leslie Greengard and June-Yub Lee. “Accelerating the non-uniform fast Fourier transform”. In: *SIAM review* 46.3 (2004), pp. 443–454.
- [13] June-Yub Lee and Leslie Greengard. “The type III non-uniform FFT and its applications”. In: *Journal of Computational Physics* 206.1 (2005), pp. 1–5.
- [14] Diego Ruiz-Antolin and Alex Townsend. “A non-uniform fast Fourier transform based on low rank approximation”. In: *SIAM Journal on Scientific Computing* 40.1 (2018), A529–A547.
- [15] Heather Wilber, Ethan N. Epperly, and Alex H. Barnett. “Superfast Direct Inversion of the Non-uniform Discrete Fourier Transform via Hierarchically Semiseparable Least Squares”. In: *SIAM Journal on Scientific Computing* 47.3 (2025), A1702–A1732.
- [16] Yingzhou Li and Jingyu Liu. *A Superfast Direct Solver for Type-III Inverse Nonuniform Discrete Fourier Transform*. 2025. arXiv: [2512.03733 \[math.NA\]](https://arxiv.org/abs/2512.03733).
- [17] Dan Coppersmith. *An approximate Fourier transform useful in quantum factoring*. 2002. arXiv: [quant-ph/0201067 \[quant-ph\]](https://arxiv.org/abs/quant-ph/0201067).
- [18] Michael A Nielsen and Isaac Chuang. *Quantum Computation and Quantum Information*. American Association of Physics Teachers, 2002.
- [19] Lin Lin. *Lecture Notes on Quantum Algorithms for Scientific Computation*. 2022. arXiv: [2201.08309 \[quant-ph\]](https://arxiv.org/abs/2201.08309).
- [20] Peter W. Shor. “Polynomial-time algorithms for prime factorization and discrete logarithms on a quantum computer”. In: *SIAM review* 41.2 (1999), pp. 303–332.
- [21] Alexei Y. Kitaev. *Quantum measurements and the Abelian Stabilizer Problem*. 1995. arXiv: [quant-ph/9511026 \[quant-ph\]](https://arxiv.org/abs/quant-ph/9511026).
- [22] Aram W. Harrow, Avinatan Hassidim, and Seth Lloyd. “Quantum algorithm for linear systems of equations”. In: *Physical review letters* 103.15 (2009), p. 150502.
- [23] Daniel S. Abrams and Seth Lloyd. “Quantum algorithm providing exponential speed increase for finding eigenvalues and eigenvectors”. In: *Physical Review Letters* 83.24 (1999), p. 5162.
- [24] Thomas G. Draper. *Addition on a Quantum Computer*. 2000. arXiv: [quant-ph/0008033 \[quant-ph\]](https://arxiv.org/abs/quant-ph/0008033).
- [25] Lidia Ruiz-Perez and Juan Carlos Garcia-Escartin. “Quantum arithmetic with the quantum Fourier transform”. In: *Quantum Information Processing* 16.6 (2017), p. 152.
- [26] Philipp Pfeffer. *Multidimensional Quantum Fourier Transformation*. 2023. arXiv: [2301.13835 \[quant-ph\]](https://arxiv.org/abs/2301.13835).
- [27] Yunseong Nam, Yuan Su, and Dmitri Maslov. “Approximate quantum Fourier transform with $O(n \log n)$ T gates”. In: *NPJ Quantum Information* 6.1 (2020), p. 26.
- [28] Elisa Bäumer, David Sutter, and Stefan Woerner. *Approximate Quantum Fourier Transform in Logarithmic Depth on a Line*. 2025. arXiv: [2504.20832 \[quant-ph\]](https://arxiv.org/abs/2504.20832).
- [29] Yuwei Jin, Xiangyu Gao, Minghao Guo, Henry Chen, Fei Hua, Chi Zhang, and Eddy Z. Zhang. “Optimizing quantum fourier transformation kernels for modern NISQ and FT architectures”.

- In: *SC24: International Conference for High Performance Computing, Networking, Storage and Analysis*. IEEE. 2024, pp. 1–15.
- [30] Berend Klaver, Stefan Rombouts, Michael Fellner, Anette Messinger, Kilian Ender, Katharina Ludwig, and Wolfgang Lechner. *SWAP-less Implementation of Quantum Algorithms*. 2024. arXiv: [2408.10907 \[quant-ph\]](#).
- [31] Hayato Goto. “Resource requirements for a fault-tolerant quantum Fourier transform”. In: *Physical Review A* 90.5 (2014), p. 052318.
- [32] Guang H. Low and Isaac L. Chuang. “Optimal Hamiltonian Simulation by Quantum Signal Processing”. In: *Physical Review Letters* 118.1 (Jan. 2017).
- [33] András Gilyén, Yuan Su, Guang H. Low, and Nathan Wiebe. “Quantum singular value transformation and beyond: exponential improvements for quantum matrix arithmetics”. In: *Proceedings of the 51st Annual ACM SIGACT Symposium on Theory of Computing*. STOC ’19. ACM, June 2019.
- [34] Andrew M. Childs and Nathan Wiebe. “Hamiltonian Simulation Using Linear Combinations of Unitary Operations”. In: *Quantum Information and Computation* 12 (2012), pp. 901–924.
- [35] Laszlo Gyongyosi and Sandor Imre. *An Improvement in Quantum Fourier Transform*. 2012. arXiv: [1207.4464 \[quant-ph\]](#).
- [36] Amir Fijany and Colin P. Williams. “Quantum wavelet transforms: Fast algorithms and complete circuits”. In: *NASA international conference on quantum computing and quantum communications*. Springer. 1998, pp. 10–33.
- [37] Mohsen Bagherimehrab and Alán Aspuru-Guzik. “Efficient quantum algorithm for all quantum wavelet transforms”. In: *Quantum Science and Technology* 9.3 (2024), p. 035010.
- [38] Julien Zylberman. *Fast Laplace transforms on quantum computers*. 2024. arXiv: [2412.05173 \[quant-ph\]](#).
- [39] Akash Kumar Singh, Ashish Kumar Patra, Anurag K. S. V., Sai Shankar P., Ruchika Bhat, and Jaiganesh G. *A Polylogarithmic-Time Quantum Algorithm for the Laplace Transform*. 2025. arXiv: [2512.17980 \[quant-ph\]](#).
- [40] Nitin Jha and Abhishek Parakh. *Quantum Hilbert Transform*. 2025. arXiv: [2505.23581 \[quant-ph\]](#).
- [41] Henry Zhang and Joseph Li. *Efficient Quantum Circuits for the Hilbert Transform*. 2026. arXiv: [2601.10876 \[quant-ph\]](#).
- [42] Andreas Klappenecker and Martin Rotteler. “Discrete cosine transforms on quantum computers”. In: *Proceedings of the 2nd International Symposium on Image and Signal Processing and Analysis*. IEEE. 2001, pp. 464–468.
- [43] Artyom M. Grigoryan, Alexis A. Gomez, and Sos S. Aghaian. “New method of computing the quantum cosine transforms”. In: *Multimodal Image Exploitation and Learning 2025*. Vol. 13457. SPIE. 2025, pp. 93–102.
- [44] Chelsea A. Williams, Annie E. Paine, Hsin-Yu Wu, Vincent E. Elfving, and Oleksandr Kyriienko. *Quantum Chebyshev Transform: Mapping, Embedding, Learning and Sampling Distributions*. 2023. arXiv: [2306.17026 \[quant-ph\]](#).
- [45] Siddhartha Jain, Vishnu Iyer, Rolando D. Somma, Ning Bao, and Stephen P Jordan. *Efficient Quantum Hermite Transform*. 2025. arXiv: [2510.04929 \[quant-ph\]](#).
- [46] Steven A. Cuccaro, Thomas G. Draper, Samuel A. Kutin, and David P. Moulton. *A new quantum ripple-carry addition circuit*. 2004. arXiv: [quant-ph/0410184 \[quant-ph\]](#).
- [47] Thomas G. Draper, Samuel A. Kutin, Eric M. Rains, and Krysta M. Svore. “A logarithmic-depth quantum carry-lookahead adder”. In: *Quantum Information and Computation* 6.4 (July 2006), pp. 351–369.
- [48] Alex Parent, Martin Roetteler, and Michele Mosca. *Improved reversible and quantum circuits for Karatsuba-based integer multiplication*. 2017. arXiv: [1706.03419 \[quant-ph\]](#).
- [49] Craig Gidney. *Asymptotically Efficient Quantum Karatsuba Multiplication*. 2019. arXiv: [1904.07356 \[quant-ph\]](#).

- [50] Mehdi Ramezani, Morteza Nikaeen, Farnaz Farman, Seyed Mahmoud Ashrafi, and Alireza Bahrampour. “Quantum multiplication algorithm based on the convolution theorem”. In: *Physical Review A* 108.5 (2023), p. 052405.
- [51] Iain Burge, Michel Barbeau, and Joaquin Garcia-Alfaro. *Quantum CORDIC – Arcsin on a Budget*. 2024. arXiv: [2411.14434](https://arxiv.org/abs/2411.14434) [quant-ph].
- [52] Junaid Aftab and Haizhao Yang. “Approximating Korobov functions via quantum circuits”. In: *Communications in Mathematical Sciences* 23.8 (2025), pp. 2077–2101.
- [53] Junaid Aftab, Christoph Schwab, Haizhao Yang, and Jakob Zech. *Quantum Circuit Encodings of Polynomial Chaos Expansions*. Submitted to *Quantum*. 2025. arXiv: [2506.01811](https://arxiv.org/abs/2506.01811) [math.NA].
- [54] Andrew M. Childs and Nathan Wiebe. “Hamiltonian Simulation Using Linear Combinations of Unitary Operations”. In: *Quantum Information and Computation* 12 (2012), pp. 901–924.
- [55] Adenilton J. da Silva and Daniel K. Park. “Linear-depth quantum circuits for multiqubit controlled gates”. In: *Phys. Rev. A* 106 (4 Oct. 2022), p. 042602.
- [56] George N. Watson. *A treatise on the theory of Bessel functions*. The University Press, 1922.
- [57] Milton Abramowitz and Irene A. Stegun. *Handbook of Mathematical Functions*. US Government Printing Office, 1964.
- [58] Junaid Aftab. *Non-Uniform-QFT*. <https://github.com/Junaid-Aftab/Non-Uniform-QFT>. 2026.

DEPARTMENT OF MATHEMATICS, UNIVERSITY OF MARYLAND, COLLEGE PARK, MD 20742, USA
Email address: junaida@umd.edu

DEPARTMENT OF STATISTICS, UNIVERSITY OF CHICAGO, IL 60637, USA
Email address: yuehaw.khoo@uchicago.edu

DEPARTMENTS OF MATHEMATICS AND COMPUTER SCIENCE, UNIVERSITY OF MARYLAND, COLLEGE PARK, MD 20742, USA
Email address: haizhao.yang@umd.edu